Chemical Geology 578 (2021) 120318

Contents lists available at ScienceDirect

Chemical Geology

journal homepage: www.elsevier.com/locate/chemgeo

Invited Research Article

Instrumental mass fractionation during sulfur isotope analysis by secondary ion mass spectrometry in natural and synthetic glasses

Z. Taracsák [a,b,*], D.A. Neave [a,c], P. Beaudry [d], J. Gunnarsson-Robin [e], R. Burgess [a], M. Edmonds [f], S.A. Halldórsson [e], M-A. Longpré [g,h], S. Ono [d], E. Ranta [e], A. Stefánsson [e], A.V. Turchyn [f], EIMF [i], M.E. Hartley [a]

[a] Department of Earth and Environmental Sciences, University of Manchester, Oxford Road, M13 9PL, United Kingdom
[b] Department of Earth Sciences, University of Oxford, South Parks Road, OX1 3AN, United Kingdom
[c] Institut für Mineralogie, Leibniz Universität Hannover, Callinstrasse 3, 30167 Hannover, Germany
[d] Department of Earth, Atmospheric and Planetary Sciences, Massachusetts Institute of Technology, Cambridge, MA 02139, USA
[e] Nordic Volcanological Center, Institute of Earth Sciences, University of Iceland, Askja, Sturlugata 7, 101 Reykjavik, Iceland
[f] Department of Earth Sciences, University of Cambridge, Downing Street, Cambridge CB2 3EQ, United Kingdom
[g] School of Earth and Environmental Sciences, Queens College, City University of New York, Flushing, NY 11367, USA
[h] The Graduate Center, City University of New York, New York, NY 10016, USA
[i] Edinburgh Ion Microprobe Facility, School of GeoSciences, University of Edinburgh, James Hutton Road, EH9 3FE, United Kingdom

ARTICLE INFO

Editor: Balz Kamber

Keywords:
Sulfur isotopes
Matrix effect
SIMS
Silicate glass
Instrumental mass fractionation

ABSTRACT

Sulfur isotope ratios are among the most commonly studied isotope systems in geochemistry. While sulfur isotope ratio analyses of materials such as bulk rock samples, gases, and sulfide grains are routinely carried out, in-situ analyses of silicate glasses such as those formed in magmatic systems are relatively scarce in the literature. Despite a number of attempts in recent years to analyse sulfur isotope ratios in volcanic and experimental glasses by secondary ion mass spectrometry (SIMS), the effects of instrumental mass fractionation (IMF) during analysis remain poorly understood. In this study we use more than 600 sulfur isotope analyses of nine different glasses to characterise the matrix effects that arise during sulfur isotope analysis of glasses by SIMS. Samples were characterised for major element composition, sulfur content, and sulfur isotope ratios by independent methods. Our glasses contain between 500 and 3400 ppm sulfur and cover a wide compositional range, including low-silica basanite, rhyolite, and phonolite, allowing us to investigate composition-dependent IMF. We use SIMS in multi-collection mode with a Faraday cup/electron multiplier detector configuration to achieve uncertainty of 0.3‰ to 2‰ (2σ) on measured $\delta^{34}S$. At high sulfur content, the analytical error of our SIMS analyses is similar to that of bulk analytical methods, such as gas-source isotope ratio mass spectrometry. We find IMF causes an offset of −12‰ to +1‰ between bulk sulfur isotope ratios and those measured by SIMS. Instrumental mass fractionation correlates non-linearly with glass sulfur contents and with a multivariate regression model combining glass Al, Na, and K contents. Both ln(S) and Al-Na-K models are capable of predicting IMF with good accuracy: 84% (ln(S)) and 87% (Al-Na-K) of our analyses can be reproduced within 2σ combined analytical uncertainty after a correction for composition-dependent IMF is applied. The process driving IMF is challenging to identify. The non-linear correlation between glass S content and IMF in our dataset resembles previously documented correlation between glass H_2O abundance and IMF during D/H ratio analyses by SIMS, and could be attributed to changes in $^{32}S^-$ and $^{34}S^-$ ion yields with changing S content and glass composition. However, a clear correlation between S ion yields and S content cannot be identified in our dataset. We speculate that accumulation of alkalis at the SIMS crater floor may be the principal driving force of composition-dependent IMF. Nonetheless, other currently unknown factors could also influence IMF observed during S isotope ratio analyses of glasses by SIMS. Our results demonstrate that the use of multiple, well-characterised standards with a wide compositional range is required to calibrate SIMS instruments prior to sulfur isotope analyses of unknown silicate glasses. Matrix effects related to glass Al-Na-K contents are of particular importance for felsic systems, where alkali and aluminium contents can vary considerably more than in mafic magmas.

* Corresponding author at: Department of Earth Sciences, University of Oxford, South Parks Road, OX1 3AN, United Kingdom.
E-mail address: zoltan.taracsak@earth.ox.ac.uk (Z. Taracsák).

https://doi.org/10.1016/j.chemgeo.2021.120318
Received 30 September 2020; Received in revised form 5 May 2021; Accepted 6 May 2021
Available online 11 May 2021

1. Introduction

Sulfur, along with hydrogen and carbon, is one of the most abundant volatile elements present in magmatic systems and strongly influences a number of processes in melts and associated fluids. It controls enrichment processes in various ore deposits at ocean floors and in magmatic hydrothermal systems (e.g. Seo et al., 2009; Simon and Ripley, 2011), and plays a key role in modulating magmatic redox conditions during melt evolution and degassing (e.g. Marini et al., 2011; Moussallam et al., 2016; Moussallam et al., 2019; Longpré et al., 2017). Sulfur bearing gases formed during magma degassing, such as H_2S and SO_2, are major constituents of many volcanic plumes and can pose a significant hazard to life due to their highly toxic nature. Understanding how sulfur behaves in magmatic systems from the melt source to the surface is essential if we are to provide better estimates on volcanic sulfur budgets and determine the source of sulfur in magmatic and hydrothermal systems. Analytical instruments such as electron probe microanalysers (EPMA) and secondary ion mass spectrometers (SIMS) are widely used to quantify sulfur contents in glasses down to a few ppm (Nash et al., 2019), and bulk-rock analysis of sulfur and its isotopes is a relatively routine procedure using ion chromatography (e.g. Michel and Villemant, 2003) and mass spectrometry (e.g. Ono et al., 2012). However, microanalyses of sulfur isotopes (we use the term sulfur isotope ratio to refer exclusively to $^{34}S/^{32}S$ ratio) in glasses are relatively scarce in the literature. Early attempts included a few analyses from Hawaiian (Hauri, 2002) and Canary Islands glasses (Gurenko et al., 2001). In the last decade a few attempts were made to determine sulfur isotopic ratios in melt inclusions, matrix glasses (Black et al., 2014; Beaudry et al., 2018), and experimentally produced silicate glasses (Fiege et al., 2014). Such datasets have the potential to provide valuable insights into sulfur degassing in magmas, during which sulfur isotopes fractionate efficiently. Sulfur isotope fractionation during degassing is a composition, temperature, and oxygen fugacity dependent process (e.g. Marini et al., 2011; Liotta et al., 2012; Fiege et al., 2014), therefore, sulfur isotope ratio analyses of glasses could be used as an effective tool to characterise fractionation processes and to link melt sulfur isotope composition to those measured in volcanic gases (e.g. de Moor et al., 2013). Sulfur isotope ratio analyses in glasses could provide further insight into sulfide ore formation in various geological settings and the large-scale and/or long-term geochemical cycle of sulfur on Earth (Farquhar et al., 2002; Evans, 2012; Jégo and Dasgupta, 2014; Walters et al., 2020).

By convention, sulfur stable isotope ratios are expressed as $\delta^{34}S$ (in ‰), calculated as

$$\delta^{34}S(‰) = \left(\left(^{34}S/^{32}S\right)_{unk} \Big/ \left(^{34}S/^{32}S\right)_{V-CDT} - 1\right) * 1000 \quad (1)$$

where $^{34}S/^{32}S_{unk}$ is the sulfur isotope ratio measured in the unknown and $^{34}S/^{32}S_{V-CDT}$ is the sulfur isotope ratio of the V-CDT standard ($^{34}S/^{32}S = 0.0441626$, Ding et al., 2001). Microanalysis of any isotope ratio requires the use of a calibrated micro-analytical tool. One of the most commonly used technique for isotope microanalysis in Earth sciences is SIMS. It is well documented that isotope analysis in glasses by SIMS is complicated by compositional matrix effects (also called instrumental mass fractionation, IMF) for many isotope systems, including hydrogen (Hauri et al., 2006), boron (Rosner et al., 2008), oxygen (Eiler et al., 1997; Hartley et al., 2012), and chlorine (Manzini et al., 2017). Recently Shimizu et al. (2019) provided details of a SIMS analytical procedure for the analyses of hydrogen and sulfur isotope ratios in basaltic glasses and noted the need of further analytical work to characterise matrix effects during S isotope ratio analyses. The development of accurate and precise methods for isotope ratio microanalysis is of particular importance for melt inclusion studies, where the desired analytical volume is extremely small.

To investigate the effect of silicate glass chemistry on S isotope ratios measured by SIMS, we require a set of glasses whose bulk $\delta^{34}S$ values have been accurately and precisely measured using an independent method. These glasses should also cover a wide range of compositions and bulk sulfur contents. Most natural volcanic samples do not fit these criteria as magmas tend to degas most of their sulfur during decompression, with only a few hundred ppm sulfur remaining dissolved in the silicate melt by the time of eruption. Furthermore, natural glasses are often compositionally heterogeneous and unsuitable for use as standards. However, some natural glasses, such as products of submarine and subglacial eruptions, can retain relatively high S contents. Experimentally produced glasses made in a high pressure and temperature apparatus offer alternative means to obtain homogeneous materials with bulk sulfur contents up to several thousands of ppm. The sulfur isotope ratio in experimental charges can be determined the same way as for bulk rocks, using gas-source isotope ratio mass spectrometry (GS-IRMS) after chemical extraction of sulfur. However, experiments typically produce only small volumes of material, which complicates bulk analysis and assessment of internal homogeneity.

Here we use six new experimental and three natural glasses, which we have analysed for major element compositions and sulfur isotope ratios, to investigate composition-dependent IMF during sulfur isotope ratio analysis of glasses by SIMS. Using glass chemistry and physical parameters, such as glass density, we perform simple linear, non-linear, and multivariate regression modelling to determine which parameters correlate with observed IMF. The best possible approach to sulfur isotope ratio analysis in glasses using SIMS is discussed based on the results of the statistical modelling. We emphasise the importance of calibrating with a range of standards covering the compositional range of the unknown silicate glasses before and during sulfur isotope ratio measurements by SIMS.

2. Glasses used for sulfur isotope ratio analysis and IMF calibration

We have used a set of nine glasses to investigate composition-dependent IMF (Fig. 1). Three of the glasses (A35, A36, and STAP) are chemically homogeneous, subglacially erupted, natural basalts from Iceland containing 500–1600 ppm sulfur, previously analysed for noble gas and nitrogen isotope ratios (Füri et al., 2010; Halldórsson et al., 2016b). Additional data on STAP and A35 are reported in Halldórsson et al. (2016a). The remaining six glasses are synthetic, and were melted under high pressure to keep sulfur dissolved in the glass. These synthetic glasses were made using powders of natural rock samples as opposed to a mixture of pure oxides and are therefore representative of natural magma compositions. The natural rock samples were selected to cover as wide a range of chemical compositions as possible (Fig. 1). Back-scattered electron images of all the nine glasses, both in low and high magnification, are provided in the supplementary material.

2.1. Experimental procedures for synthetic glasses

Synthetic, sulfur-bearing glasses were produced using an internally heated pressure vessel (IHPV) at the Leibniz Universität Hannover. Starting materials included two lava samples from the Canary Islands (Mg-rich basanite TNR14–01 and low-Mg basanite EGT17–01), two lava samples from Lacher See, Eifel Volcanic Field (nephelinite LS-17980 and phonolite LS-17985), one lava sample from Hawaii (picrite HAW-16095), and an obsidian from Lipari (LIP-17714). Glass major element compositions are presented in Fig. 1 and Table 1.

Samples were first ground into powders, then melted at 1200 to 1400 °C in a 1-atm furnace and quenched into glass to produce a homogeneous, devolatilised material. The glasses were powdered again, and doped with various amounts of $CaSO_4$ with known sulfur isotopic composition ($\delta^{34}S = 11.1 \pm 0.4$‰, see analytical techniques section). The mix was dried in a furnace at 500 °C for 3 h to remove adsorbed water.

Between 132 and 185 mg of the sample powders were placed in $Au_{80}Pd_{20}$ capsules, along with 6–7 mg of H_2O, corresponding to 4 to 4.5

wt% H_2O content. The addition of water was required to lower the sample liquidus temperatures and to set fO_2 conditions to highly oxidising (~FMQ+4, Botcharnikov et al., 2005) to prevent sulfide saturation and sulfur loss to capsules. IHPV experiments were carried out at 1300 °C and 300 MPa using an Ar pressure medium. The duration of experiments was two hours, after which capsules were drop-quenched onto a room-temperature Cu plate while still under pressure. Capsules were then opened with a diamond saw and the glass was gently crushed and removed from the capsules using pliers. Smaller chips were used for bulk $\delta^{34}S$ analyses, while larger chips were set aside to be used for SIMS analyses.

3. Analytical techniques

Major, minor element, and sulfur contents of synthetic and natural glasses were measured using a Cameca SX100 electron microprobe (EPMA) at the University of Manchester. The following standards were used during glass analyses, with on-peak counting times in parentheses: Si (40 s), Na (80 s), and Al (80 s): jadeite; Ca (30 s): wollastonite; Mg (80 s): periclase; Cl (30 s): sodalite; S (40 s): anhydrite; P (30 s): apatite; K (30 s): potassic feldspar; Ti (30 s): rutile; Mn (80 s); tephroite; Fe (80 s): fayalite. Beam current was set at 3 nA for Si to avoid detector oversaturation, resulting in 330 and 720 cps/nA signal and an average 1.4 wt % counting statistic error (2σ) on SiO_2 contents. Other elements were measured using a 20 nA beam current. Beam diameter was set at 15 μm. A time-dependent intensity correction was applied for Na to account for loss due to volatilisation. Analytical error of measured S contents, based on counting statistics of the measured signal, was between 100 and 130 ppm, while the standard deviation of multiple measurements on various glass chips was between 90 and 170 ppm (2σ).

Glass $S^{6+}/\sum S$ ratios were measured using the same EPMA. As the position of the $S_{K\alpha}$ peak changes linearly depending on the oxidation state of S in glass (Carroll and Rutherford, 1988), the $S^{6+}/\sum S$ ratio of glasses can be determined by either scanning over the $S_{K\alpha}$ peak or by fixing spectrometers at the maximum intensity of S^{2-} and S^{6+} and measuring the ratio of the two intensities; this type of $S^{6+}/\sum S$ analyses is commonly known as the peak-shift method. Instead of the more widely used peak scanning method, we used a fixed spectrometer position method. The S^{2-} (61414) and the S^{6+} (61445) peak positions were determined by scanning over a pyrite and an anhydrite standard,

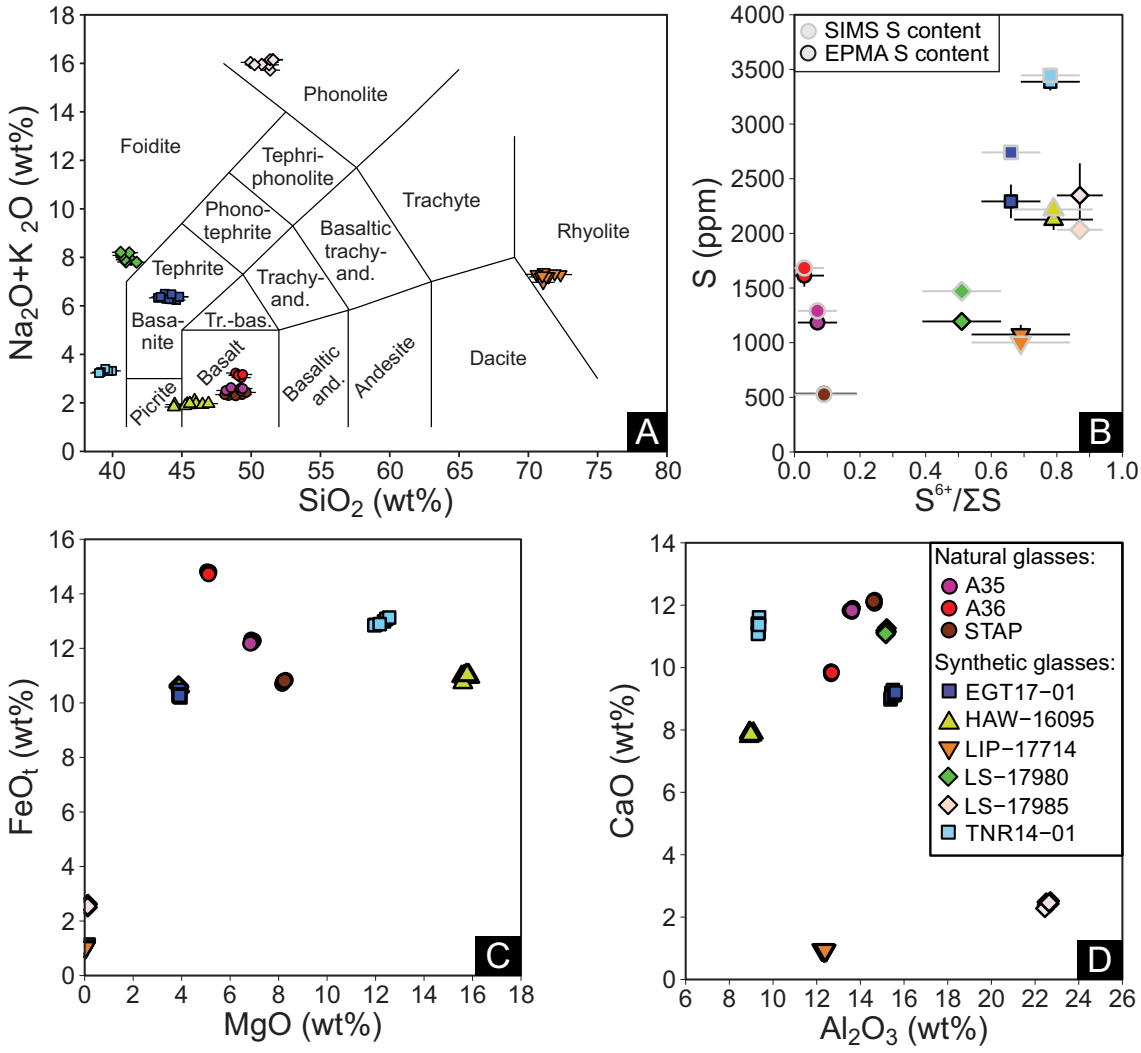

Fig. 1. (A) Compositions of synthetic and natural glasses used as prospective standards during sulfur isotope ratio analyses on a total alkali vs. silica diagram (Le Bas et al., 1986). Most glasses are mafic in composition apart from a rhyolite (LIP-17714) and a phonolite (LS-19785). (B) Sulfur content of the glasses vs. $S^{6+}/\sum S$ ratio: synthetic glasses are dominated by oxidised S^{6+} while natural glasses are more reduced and contain mostly S^{2-}. Symbols with black outlines are EPMA data, while grey outlines are SIMS-based S measurements quantified using $^{18}O^-$ relative ion yields of $^{32}S^-$. The difference between EPMA and SIMS data for EGT17–01 and LS-17980 is likely due to the peak shift of the S K_α peak for glasses containing mixed valence S, resulting in low EPMA-based S contents. (C) Total FeO vs. MgO and (D) CaO vs. Al_2O_3 diagrams indicate the glasses cover a wide compositional range for these elements. Error bars are 1σ standard deviations.

Table 1
Compositions of synthetic and natural glasses. Values are in wt% if not otherwise stated. Icelandic glass $Fe^{3+}/\sum Fe$ ratios are based on data from Óskarsson et al. (1994) and Shorttle et al. (2015). Sulfur contents shown in the table include those measured by EPMA, SIMS, and SIMS cps, the latter being calculated from ^{32}S cps/nA (see Results section for more detail). Values for $\Delta^{33}S$ and $\Delta^{36}S$ in A35, A36, and STAP are reported relative to laboratory SF_6 reference gas SG-1 (the anchoring of $\Delta^{33}S$ and $\Delta^{36}S$ values to the V-CDT scale are detailed in Ranta et al. (n.d.). For experimental glasses, $\Delta^{33}S$ and $\Delta^{36}S$ values were quantified the same way as described in Fortin et al. (2019). Uncertainty given in every even column is 2σ.

Sample	A36		STAP		A35		LS-17980		HAW-16095		TNR14–01		LS-17985		EGT17–01		LIP-17714	
Type	Natural glass		Natural glass		Natural glass		Synthetic gl.		Synthetic gl.		Synthetic gl.		Synthetic gl.		Synthetic gl.		Synthetic gl.	
	AVG	2σ	AVG	2σ	AVG	2σ	AVG	2σ	AVG	2σ	AVG	2σ	AVG	2σ	AVG	2σ	AVG	2σ
SiO_2	**49.1**	*0.4*	**48.9**	*1.3*	**48.9**	*1.1*	**41.0**	*0.7*	**45.6**	*1.6*	**39.5**	*0.7*	**51.0**	*0.6*	**44.1**	*1.1*	**71.3**	*1.0*
TiO_2	**3.050**	*0.007*	**1.620**	*0.035*	**1.645**	*0.019*	**2.355**	*0.046*	**1.889**	*0.025*	**3.937**	*0.033*	**0.290**	*0.005*	**3.162**	*0.056*	**0.064**	*0.015*
Al_2O_3	**12.67**	*0.03*	**14.63**	*0.06*	**13.60**	*0.11*	**15.18**	*0.07*	**8.98**	*0.13*	**9.33**	*0.05*	**22.60**	*0.09*	**15.48**	*0.15*	**12.34**	*0.14*
FeO(t)	**14.78**	*0.07*	**10.79**	*0.10*	**12.24**	*0.12*	**10.58**	*0.13*	**10.96**	*0.17*	**12.97**	*0.24*	**2.58**	*0.06*	**10.32**	*0.17*	**1.07**	*0.10*
FeO	**11.82**		**8.63**		**9.79**		**3.26**		**4.22**		**4.41**		**0.82**		**4.38**		**0.50**	
Fe_2O_3	**3.28**		**2.40**		**2.72**		**8.14**		**7.49**		**9.51**		**1.96**		**6.60**		**0.64**	
MnO	**0.24**	*0.02*	**0.19**	*0.018*	**0.21**	*0.015*	**0.30**	*0.015*	**0.16**	*0.017*	**0.18**	*0.019*	**0.23**	*0.012*	**0.21**	*0.012*	**0.04**	*0.010*
MgO	**5.10**	*0.068*	**8.22**	*0.109*	**6.89**	*0.101*	**3.89**	*0.057*	**15.73**	*0.218*	**12.24**	*0.497*	**0.12**	*0.003*	**3.90**	*0.044*	**0.03**	*0.010*
CaO	**9.85**	*0.07*	**12.11**	*0.09*	**11.85**	*0.10*	**11.15**	*0.14*	**7.87**	*0.08*	**11.29**	*0.41*	**2.43**	*0.07*	**9.14**	*0.17*	**0.94**	*0.03*
Na_2O	**2.74**	*0.14*	**2.06**	*0.12*	**2.37**	*0.12*	**4.55**	*0.29*	**1.57**	*0.14*	**2.32**	*0.18*	**7.69**	*0.22*	**4.51**	*0.14*	**3.33**	*0.24*
K_2O	**0.41**	*0.006*	**0.28**	*0.010*	**0.19**	*0.008*	**3.44**	*0.041*	**0.38**	*0.016*	**0.99**	*0.097*	**8.32**	*0.178*	**1.85**	*0.059*	**3.90**	*0.056*
P_2O_5	**0.32**	*0.060*	**0.21**	*0.042*	**0.15**	*0.045*	**1.15**	*0.062*	**0.20**	*0.030*	**0.69**	*0.047*	**0.05**	*0.015*	**1.24**	*0.086*	**0.01**	*0.020*
S (ppm, EPMA)	**1614**	*202*	**534**	*74*	**1184**	*104*	**1194**	*125*	**2126**	*190*	**3387**	*160*	**2347**	*588*	**2292**	*308*	**1075**	*177*
S (ppm, SIMS RIY)	**1683**	*0*	**526**	*0*	**1291**	*4*	**1471**	*46*	**2219**	*45*	**3446**	*8*	**2033**	*28*	**2741**	*15*	**1002**	*23*
S (ppm, SIMS cps)	**1581**	*158*	**487**	*37*	**1206**	*61*	**1598**	*306*	**2222**	*309*	**3806**	*902*	**1888**	*284*	**2740**	*254*	**871**	*184*
F (ppm)	**970**	*4*	**724**	*2*	**488**	*6*	**165**	*3*	**12**	*1*	**295**	*1*	**102**	*1*	**1212**	*9*	**102**	*0*
Cl (ppm, EPMA)	**150**	*88*	**181**	*84*	**87**	*58*	**142**	*57*	**7**	*82*	**26**	*69*	**933**	*57*	**138**	*63*	**110**	*89*
Cl (ppm, SIMS)	**202**	*2*	**226**	*1*	**86**	*1*	**153**	*4*	**27**	*2*	**43**	*2*	**965**	*14*	**153**	*2*	**143**	*1*
H_2O (SIMS)	**0.71**	0.009	**0.34**	0.002	**0.30**	0.008	**4.24**	*0.012*	**4.74**	*0.022*	**4.68**	*0.003*	**4.87**	*0.05*	**4.17**	*0.006*	**4.57**	*0.018*
H_2O (FTIR)	**0.70**	*0.09*	**0.37**	*0.09*	**0.28**	*0.04*	**3.37**	*1.20*	**2.66**	*0.61*	**5.65**	*1.75*						
CO_2 (ppm)	**586**	*1464*	**48**	*7*	**159**	*70*	**1141**	*22*	**1216**	*10*	**870**	*12*	**277**	*17*	**695**	*24*	**233**	*80*
Total	**99.32**		**99.59**		**98.64**		**98.66**		**98.82**		**99.09**		**100.42**		**98.77**		**97.66**	
$Fe^{3+}/\Sigma Fe$	**0.15**		**0.13**		**0.15**		**0.69**	*0.03*	**0.61**	*0.03*	**0.66**	*0.03*	**0.68**	*0.02*	**0.58**	*0.03*	**0.54**	*0.08*
$S^{6+}/\Sigma S$	**0.03**	*0.11*	**0.09**	*0.20*	**0.07**	*0.12*	**0.51**	*0.24*	**0.79**	*0.24*	**0.78**	*0.17*	**0.87**	*0.07*	**0.66**	*0.19*	**0.69**	*0.29*
$\delta^{34}S$ (‰)	**−0.57**	*0.91*	**−1.10**	*0.66*	**−0.36**	*0.06*	**9.38**	*0.50*	**11.28**	*0.50*	**11.58**	*0.50*	**8.76**	*0.50*	**10.96**	*0.50*	**11.96**	*0.50*
$\Delta^{33}S$ (‰)	**−0.015**	*0.037*	**−0.011**	*0.014*	**−0.014**	*0.021*	**−0.006**		**0.008**		**0.019**		**0.007**		**0.021**		**0.004**	
$\Delta^{36}S$ (‰)	**0.063**	*0.076*	**0.004**	*0.032*	**0.109**	*0.058*	**0.763**		**0.771**		**0.206**		**0.094**		**0.808**		**0.480**	

respectively. Two background positions were measured simultaneously. The background count rate was subtracted from the S^{2-} and S^{6+} peak counts. Background-subtracted count rates were then divided, and $S^{6+}/\sum S$ ratios of the glasses were calculated relative to the ratios measured on pyrite ($S^{6+}/\sum S = 0$, $S^{6+}_{peak}/S^{2-}_{peak} = 0.656 \pm 0.028$, 2σ) and anhydrite ($S^{6+}/\sum S = 1$, $S^{6+}_{peak}/S^{2-}_{peak} = 1.313 \pm 0.034$, 2σ) standards, assuming $S^{6+}/\sum S$ and $S^{6+}_{peak}/S^{2-}_{peak}$ both change linearly (Carroll and Rutherford, 1988). Compared to the more widespread peak scanning method, the fixed spectrometer method used here is faster (~60 s), hence it reduces the chance of oxidation or reduction (e.g. Wilke et al., 2011) during sample-electron beam interaction. Note that the peak-shift method applied here is generally less accurate than analyses carried out using synchrotron methods, such as X-ray absorption spectroscopy. Uncertainties of major element contents and $S^{6+}/\sum S$ ratios are provided in Table 1.

Glass $Fe^{3+}/\sum Fe$ ratios were determined using wet chemistry and colorimetry at the Leibniz Universität Hannover following the procedures described by Schuessler et al. (2008). Between 4 and 17 mg of glass was reacted with NH_4VO_3, H_2SO_4 and HF. In summary, V^{5+} oxidised Fe^{2+} originating from the glass during dissolution into Fe^{3+} by producing oxidation-resistant V^{4+}. Fe^{2+} and V^{5+} were later regenerated from Fe^{3+} and V^{4+} produced during the previous reaction by adding boric acid to the solution. Fe^{2+} was then reacted with 2:2'bipyridyl to form Fe(II)-2:2'bipyridyl, which has a strong absorption band in the visible spectrum. Absorption of Fe^{2+} was measured first by colorimetry. After the measurement of Fe^{2+}, hydroxylamine hydrochloride was added to the solution, reducing all Fe that was originally present as Fe^{3+} to Fe^{2+}. Absorption was then measured again to determine total Fe content to get $Fe^{3+}/\sum Fe$.

Three natural Icelandic glasses and three of our synthetic glasses were analysed for their H_2O contents by transmission micro-FTIR (Fourier transform infrared spectroscopy), using a Perkin Elmer Spotlight-400 instrument at the University of Manchester equipped with a mercury-cadmium-telluride (MCT) detector. We used the Beer-Lambert law to quantify H_2O contents in the samples, which requires sample thickness and molar absorptivity to be known. Glass chips were made into thin (30–120 μm) double-polished wafers. Thickness of the wafers was determined using a manual Miyamoto micrometer, which has a nominal precision of ±2 μm. Absorbance spectra of the glasses were recorded between 7000 cm^{-1} to 600 cm^{-1} to include H_2O peaks at 5200 and 1630 cm^{-1} and OH^- peaks at 4500 and 3550 cm^{-1}. Between three to eight spectra were taken from each sample. Absorbance from each spectrum was determined after manually subtracting the background from the peaks. H_2O contents were quantified using molar absorptivities taken from Mercier et al. (2010). Molar absorptivity values were varied based on the number of non-bridging oxygens per total oxygen atoms (NBO/T): for TNR14–01 molar absorptivities of 43.96, 0.56 and 0.58 were used for the 3550, 4500 and 5200 cm^{-1} peaks, respectively, while for all other mafic glasses molar absorptivities of 62.8, 0.62 and 0.67 were used. For hydrous experimental glasses, H_2O contents were calculated by adding together water contents derived from the 5200 cm^{-1} H_2O and 4500 cm^{-1} OH^- peaks. For low (<1 wt%) H_2O glasses from Iceland the water content was determined using the absorbance of the 3550 cm^{-1} peak, which was taken as total H_2O.

Sulfur isotopic composition of the anhydrite used to add sulfur to the experimental charges was measured at the Godwin Laboratory, University of Cambridge, using a Thermo Finnegan Delta V Plus GS-IRMS. Sulfur from the anhydrite was extracted as H_2S using Thode's solution, i.e. HI-H_2PO_3-HCl mixture, under a constant flow of N_2 gas. The extraction procedure took approximately three hours. H_2S was precipitated in Zn-acetate as ZnS, which was then reacted with $AgNO_3$ to form Ag_2S. The resulting Ag_2S precipitate was dried, combusted into SO_2 at 1030 °C in a flash element analyser and analysed for $\delta^{34}S$.

Bulk sulfur isotope ratios including $^{33}S/^{32}S$, $^{34}S/^{32}S$, and $^{36}S/^{32}S$ in the synthetic glasses were measured using a Thermo-electron MAT 253 GS-IRMS at Massachusetts Institute of Technology. Sample masses were between 21 and 47 mg. Total sulfur was extracted from the glass samples using tin(II)-strong phosphoric acid (Kiba reagent; Sasaki et al., 1979) under a constant flow of N_2 gas. The reaction produces H_2S, which was precipitated in Zn-acetate solution as ZnS, and was later reacted with $AgNO_3$ to form Ag_2S. The Ag_2S precipitates were then dried, placed in aluminium foil and fluorinated in nickel reaction vessels for 8 h at 300 °C using fluorine gas. The resulting SF_6 was then purified by gas chromatography, going through a column packed with 5 Å molecular sieve and HayeSep Q. Gas pressures of the purified SF_6 were measured before isotopic analysis. Repeated analyses ($n = 7$) of a mid-ocean ridge glass sample (ALV4055-B6) using the same extraction method and the same instrument indicate that a precision of ±0.5‰ (2σ) in $\delta^{34}S$ can be reached for glass samples using this extraction procedure. Repeated analyses of international reference sulfide material (IAEA-S1) have yielded $\delta^{34}S$ precisions of 0.26‰ for 2 mg Ag_2S ($n = 28$, Ono et al., 2012) and 0.82‰ (2σ) for 40–130 μg Ag_2S ($n = 13$, Fortin et al., 2019).

Bulk sulfur isotopic compositions of natural, sulfur-containing Icelandic glasses A35, A36, and STAP (Fig. 1) were measured using the same Kiba extraction procedure, carried out at the University of Iceland. Sulfur isotope ratios were determined using the same Thermo-electron MAT 253 GS-IRMS at the Massachusetts Institute of Technology as for the synthetic glasses. The larger mass of natural samples meant multiple extractions (3 to 4) could be carried out on larger amounts of extracted sulfur. Around 2 mg of the extracted Ag_2S was converted to SF_6, purified and measured using the same procedure as for the synthetic glasses. Repeated analysis of A35 ($n = 3$), A36 (n = 3) and STAP ($n = 4$) indicate 2σ reproducibility of 0.06‰, 0.91‰, and 0.66‰, respectively using the Kiba extraction method.

3.1. SIMS analytical conditions and data processing

Sulfur isotope ratios in the synthetic and natural glasses were measured by secondary ion mass spectrometry at the Edinburgh Ion Microprobe Facility (EIMF) at the University of Edinburgh in November 2019. Samples were mounted in epoxy and gold-coated prior to analysis. Sulfur isotope ratios in glasses were determined using a Cameca IMS-1270 instrument operated in multi-collection mode. A Cs^+ primary ion beam with an accelerating voltage of 10 kV and a beam current of 2–3.7 nA was used for analytical sessions 2 to 14. A smaller 0.9–1.3 nA primary beam current was used during the first analytical session. The primary beam diameter was set at 10 μm. A low-energy flood electron gun was used to compensate for positive charge build up on the sample surface. Secondary ions were accelerated with 10 kV (resulting in a total impact energy of 20 keV) from the sample surface into the mass spectrometer. Secondary ions were then passed through a 60 μm transfer lens, followed by a 400 μm contrast aperture, a 60 μm entrance slit, and finally a 2000 μm field aperture before entering the electrostatic sector of the instrument. Sulfur isotopes were analysed as $^{34}S^-$ using an ETP electron multiplier (EM) and $^{32}S^-$ using a Faraday cup (FC-L1) to optimise count rate on both isotope species, as the count rate for $^{34}S^-$ would have been too low for a FC detector at low S contents. Mass resolution was set at ~3600, which is calculated by the Cameca IMS-1270 based on instrument geometry, to distinguish between isobaric interferences on mass ~32 ($^{32}S^-$, $^{16}O_2^-$, $H^{31}P^-$) and ~34 ($^{34}S^-$, $^{33}SH^-$, $^{16}O^{18}O^-$). Based on mass spectra collected using this setup, the true mass resolution was closer to ~2000 on the FC and ~4000 on the EM detector when determined using the full width at half maximum method (Fig. 3). Before each analysis the sample surface was pre-sputtered for 60 s, followed by a secondary ion beam alignment using dynamic transfer plates. Both $^{32}S^-$ and $^{34}S^-$ ions were measured for 20 cycles, with each cycle being 4 s long. This configuration resulted in count rates of 6×10^5 to 1.17×10^7 for $^{32}S^-$ and 2.9×10^4 to 5.26×10^5 for $^{34}S^-$ per cycle, with count rate standard errors varying between 0.05 and 2.17% for both isotopes. Total analysis time, including pre-sputtering, was ~3.5 min per measurement.

Sulfur and volatile contents (H_2O, CO_2, F, Cl) of the glasses were analysed on the same instrument, using a Cs^+ primary ion beam with an

accelerating voltage of 10 kV, a beam current of ~ 1 nA, and a primary beam diameter of 10 μm. Secondary ions were accelerated by a potential of 10 kV without the use of a voltage offset energy filter. Similarly to S isotope ratio analyses, positive charge build was compensated using a flood electron gun. Prior to analyses the sample surface was pre-sputtered for 60 s. Ions of $^{12}C^-$ (2), $^{16}O^1H^-$ (0.5), $^{18}O^-$ (2), $^{19}F^-$ (4), $^{30}Si^-$ (2), $^{31}P^-$ (2), $^{32}S^-$ (4), and $^{35}Cl^-$ (4) were measured sequentially with an EM detector, using magnetic peak switching (on-peak counting times in seconds are given in parentheses). Mass positions 11.2 (0.5) and 11.5 (0.5) were also measured. The entrance slit was set at 40 μm. Analyses consisted of nine cycles. Detection limits for S and H_2O, measured in nominally H_2O (GSD-1G) and S-free glasses (StHs6/80-G and T1-G), were <80 ppm and < 4 ppm, respectively. Sulfur contents were quantified by relative ion yields (RIY) of $^{32}S^-$ compared to $^{18}O^-$, using standards NIST 620 (500 ppm S) and L17 (1320 ppm S). Water contents were quantified using a linear regression fitted between the measured $^{16}O^1H^-/^{30}Si^-$ × Si (wt%) and the H_2O content of glasses A35, A36, and STAP, which were measured by FTIR.

3.1.1. Drift, EM deadtime, and other corrections of sulfur isotope ratios

Due to the high count rate of up to 5.26 × 10^5 counts per cycle on the EM detector, a large deadtime correction was applied on the ^{34}S count rate. Deadtime correction is calculated as

$$N_{corr} = N_{meas}/(1 - N_{meas}*\tau) \quad (2)$$

where N_{corr} is the deadtime-corrected counts, N_{meas} is the uncorrected counts and τ is the deadtime (in seconds). The deadtime correction on the Cameca IMS-1270 is electronically set: during the analytical session it was determined to be 51 ns, based on instrument design. As shown in eq. 2, the size of the deadtime correction is count rate dependent, and its value changes with variable glass sulfur content. Therefore, EM deadtime was measured to test if the electronically set deadtime is correct by analysing the A35 glass (which is a glass with intermediate S content) using different entrance slit sizes, hence changing the $^{32}S^-$ and $^{34}S^-$ count rates. By regressing $^{32}S/^{34}S$ ratio against $^{32}S^-$ count rate, and using the slope and intercept of the regression, a deadtime of 47.6±0.9 ns was calculated. The difference between the electronically set and measured EM deadtime changes sulfur isotope ratios for A35 by 0.00002, equal to a difference of 0.5‰ in $\delta^{34}S$. As this change is significant with respect to analytical errors (Fig. 2), data were reprocessed using eq. 2 and the 47.6 ns deadtime.

A deadtime correction is not required for the FC detector measuring $^{32}S^-$. However, due to the electronic baseline noise of the Faraday Cup current amplifier (Fig. 3), a background correction is required for the raw $^{32}S^-$ counts. A yield correction is also applied to the measured count rates. Both of these corrections were applied for all analyses by the Cameca CIPS software.

Sulfur isotope ratio analysis of the samples was usually carried out in a sequence of 14 analyses, with each sequence consisting of four primary drift standard analyses (i.e. the glass on which analyses are carried out repeatedly during the whole session to monitor any changes in measured isotope ratios), followed by five analyses of two different glass samples. EGT17–01 was used as the primary drift standard. Analyses were carried out in 14 sessions, with a new session starting after each instance of sample exchange or beam shutdown (i.e. switching the primary accelerating voltage and the beam current off). All 14 sessions were affected by instrumental drift, evidenced by a systematic decrease in measured $^{34}S/^{32}S$ ratios in the primary drift standard. This drift is caused mainly by the EM detector ageing, which results in the loss of counts for $^{34}S^-$ as more analyses are carried out; the EM voltage was increased multiple times during the two week analytical period to compensate for this effect. A similar observation was made by Shimizu et al. (2019) during S isotope ratio analyses in mafic glasses by SIMS. For each session, instrumental drift was corrected using a linear regression procedure to restore the primary drift standard measurements to a constant sulfur isotope ratio. Further details of the drift correction procedure are provided in the supplementary material. The R^2 of the linear regressions between measured isotope ratios and analyses number varied between 0.71 and 0.99 (Fig. S1). The weaker correlations are associated with sessions where measured instrumental drift was small (<0.001 change in measured sulfur isotope ratio on the primary drift standard).

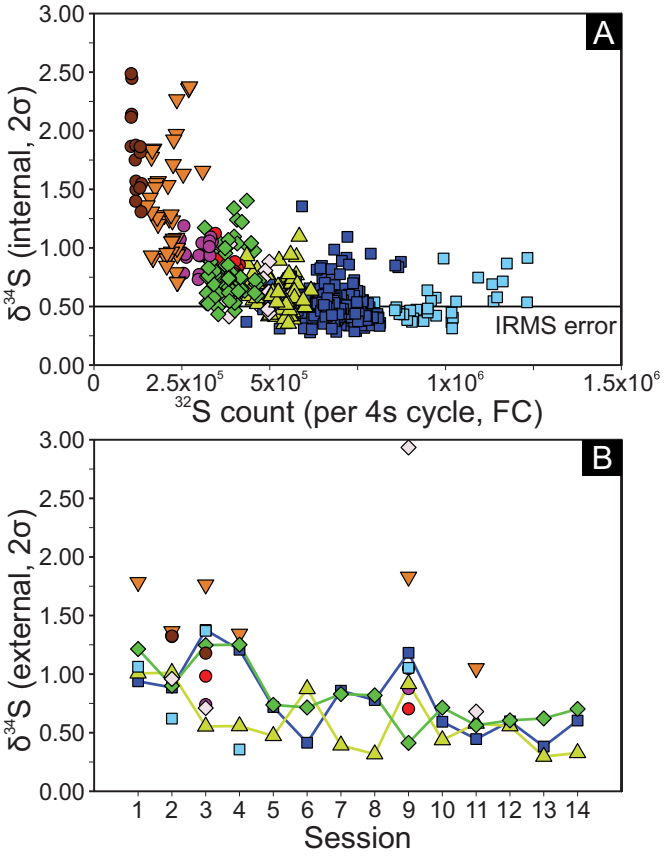

Fig. 2. Internal analytical precision plotted against $^{32}S^-$ counts (per 4 s cycle) (A) and external precision (standard deviation of drift corrected glass S isotope ratios) plotted by session (B). All errors are 2σ. At high counts (>5 × 10^5), internal precision is generally between 0.3 and 1.0‰, while at lower counts it increases, due to Poisson noise, to 2.5‰ for the most sulfur-poor glasses. External precision for primary drift standard EGT17–01 is between 0.3 and 1.4‰. The other two glasses analysed in every session, LS-17980 and HAW-16095, have similar precision to EGT17–01. Symbols are same as in Fig. 1.

3.1.2. Internal and external precisions of SIMS analyses

We use the definition of Fitzsimons et al. (2000) to determine the internal and external analytical precision of our sulfur isotope ratio analyses in glasses by SIMS. Internal analytical precision, i.e. the precision of a single analysis, is based on the counting statistics error of the 20 analytical cycles, and is calculated by the Cameca IMS-1270 instrument assuming Poisson noise. External precision is defined as the standard deviation of repeat analyses carried out on same sample during the same session: here external precision is calculated using the standard deviation of primary drift standard, EGT17–01 after drift correction is applied. Furthermore, a combined external precision can be defined, where the analytical uncertainty of the bulk $\delta^{34}S$ is also taken into account. The combined external precision is propagated using the general error propagation formula (assuming variables are independent):

$$\sigma_f = \sqrt{\left(\frac{\partial f}{\partial x}\right)^2 * \sigma_x^2 + \left(\frac{\partial f}{\partial y}\right)^2 * \sigma_y^2 + \left(\frac{\partial f}{\partial z}\right)^2 * \sigma_z^2 \ldots} \quad (3)$$

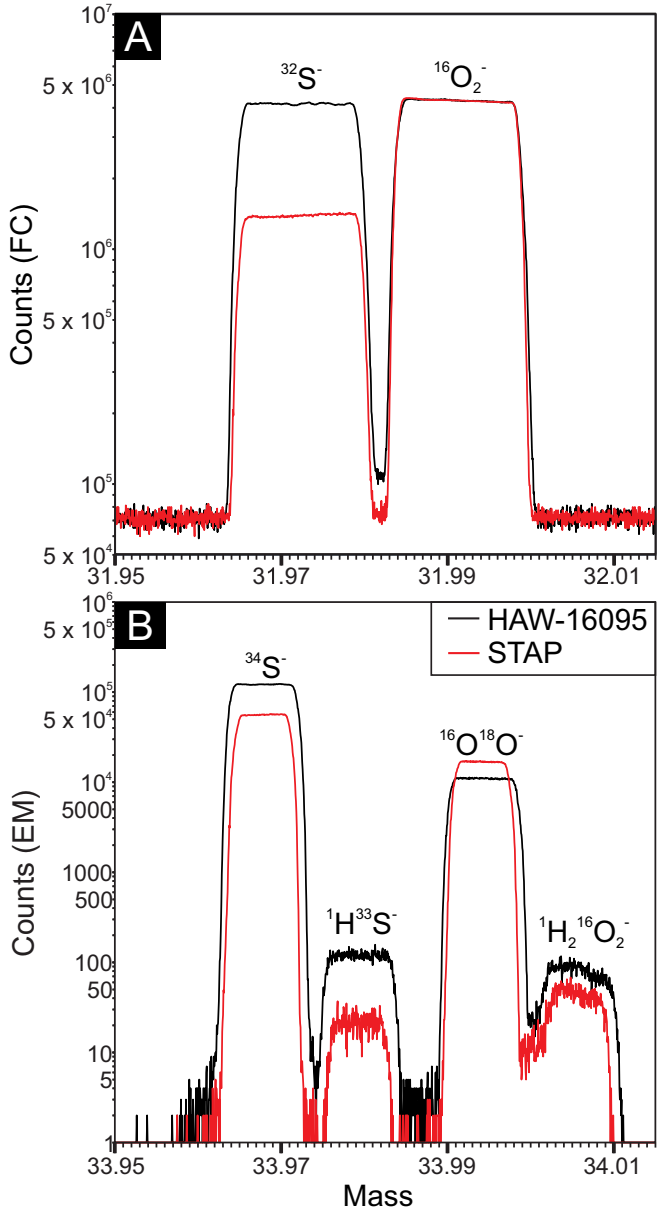

Fig. 3. Mass scans of glass standards STAP and HAW-16095 taken on the FC (A) and EM (B) detectors. On the EM all peaks are considered to be completely resolved. On the FC, the $^{16}O_2^-$ and $^{32}S^-$ peaks are resolved at <0.1% of the $^{32}S^-$ peak height for STAP, while the same two peaks are resolved at < 1% peak height in the HAW-16095 scan. A larger and more detailed figure of the same mass scans is provided in the supplementary material (Fig. S5).

where σ_f is the standard deviation of function *f*, σ_x, σ_y, and σ_z are the standard deviations of variables x, y, and z. In case of the two variables (bulk GS-IRMS data and the drift corrected SIMS data) being multiplied or divided, such as when calculating IMF (see eq. 5), eq. 3 can be simplified:

$$\sigma_{comb} = X_{drift} * \sqrt{\left(\frac{\sigma_{ext}}{X_{drift}}\right)^2 + \left(\frac{\sigma_{IRMS}}{X_{bulk}}\right)^2} \quad (4)$$

where σ_{comb} is the combined uncertainty, σ_{ext} is the external precision of the SIMS analyses measured on the primary drift standard EGT17–01 during each session, and σ_{IRMS} is the bulk error of the GS-IRMS analyses, while X_{drift} is the drift-corrected S isotope ratio of the sample, and X_{bulk} is the bulk S isotope ratio determined by GS-IRMS, all expressed as $^{34}S/^{32}S$.

Internal precision of sulfur isotope ratio analyses is primarily determined by the measured count rate and hence sulfur contents of the glass. Once the count rate on the Faraday cup for $^{32}S^-$ decreases below 5 $\times$ 10^5 the analytical error starts increasing rapidly, as at low count rates the noise of the FC detector represented a larger proportion of the measured $^{32}S^-$ counts (Fig. 2A). At higher count rates the combined uncertainty is primarily controlled by the error associated with the drift correction, which varies between 0.19 and 0.69‰. When errors associated with the drift correction are small and count rate is $> 5 \times 10^5$, the analytical uncertainty achieved by SIMS may be below 0.5‰, similar to errors associated with our GS-IRMS analyses. Our lowest combined uncertainty is less than half of the 1.6‰ reported by Black et al. (2014) for sulfur isotope ratio measurements by SIMS. Fiege et al. (2014) reported 0.52‰ reproducibility on a mid-ocean ridge basalt (MORB) glass, similar to our drift correction errors; however, they did not provide combined analytical uncertainty. Our error propagation calculations show that if the optimal conditions of high count rate and no or small instrumental drift are met, multi-collector SIMS and bulk GS-IRMS analyses have comparable analytical uncertainty during sulfur isotope ratio measurements.

4. Results

4.1. Major element composition and sulfur content of glasses

Major element composition of the glasses measured by EPMA are presented in Fig. 1 and Table 1. The three natural Icelandic glasses are all basaltic in composition, while experimental glasses cover a wider compositional range, including alkaline basalts, a phonolite, and a rhyolite. The nine glasses cover a SiO_2 range of 39.5 to 71.3 wt%. Alkali contents are also variable, with Na_2O and K_2O contents between 1.6–7.7 wt% and 0.7–8.3 wt%, respectively. Total alkali content is up to 16.0 wt % in the phonolitic glass (LS-17985). Total FeO contents of the glasses are between 1.1 and 14.8 wt% (Fig. 1C). In Icelandic glasses Fe is mainly present as Fe^{2+}: $Fe^{3+}/\sum Fe$ is 0.13 for STAP based on data provided by Óskarsson et al. (1994) for the same sample, while for A35 and A36 it was assumed to be 0.15 based on data presented by Shorttle et al. (2015) for various Icelandic glasses. Experimental glasses are considerably more oxidised, with $Fe^{3+}/\sum Fe$ ratios between 0.58 and 0.69. Glass MgO contents are between 0.03 and 17.7 wt%, covering most reasonable silicate glass compositions (Fig. 1C). Glass CaO and Al_2O_3 contents are between 0.94 and 12.1 wt% and 9.3–22.6 wt%, respectively (Fig. 1D). The H_2O content of Icelandic subglacial glasses is between 0.3 and 0.7 wt%. Based on SIMS data, synthetic glasses have 4.17 to 4.87 wt% H_2O, which is consistent with the amount of H_2O added to experimental charges. Errors associated with FTIR data collected from three synthetic glasses are large: two out of three overlap with the SIMS H_2O data, while the third glass (HAW-16095) has a lower H_2O content measured by FTIR compared to SIMS (Table 1). As the amount of water added to the capsules is consistent with the SIMS data, we accept SIMS data as the correct H_2O content, and use it later in the text for regression modelling.

Sulfur contents in the glasses, measured by EPMA, are between 534 and 3378 ppm. A similar range was measured by SIMS (526 to 3446 ppm); EPMA and SIMS S data are consistent for most glasses (Fig. 1B). A difference between EPMA and SIMS S content can be observed for EGT17–01 and LS-17980; these two glasses contain mixed valence S (Fig. 1B), resulting in a peak shift for the S K_α peak used to quantify S contents by EPMA. This shift may have moved the S K_α peak away from the detector position, resulting in an off-peak measurement, loss of counts, and consequently low measured S contents. Glass sulfur contents were also extrapolated from the SIMS $^{32}S^-$ count rates. The count rate was converted to counts per second (cps) and divided by the primary beam current to calculate $^{32}S^-$ cps/nA for each analysis. The average cps/nA measured on EGT17–01 in each session was assumed to be equal to 2741 ppm sulfur, i.e. the S content of EGT17–01 measured by SIMS

using $^{18}O^-$ relative ion yields. Standard deviation of sulfur contents measured using cps are generally higher than errors in EPMA and SIMS measurements, and cps-based sulfur contents often vary between sessions. The largest session-to-session variation is observed for TNR14–01 in cps-based S contents. For the purpose of regression analyses we use the SIMS-derived S contents of the glasses unless otherwise stated.

Sulfur speciation varies significantly among the nine glasses (Fig. 1B). Natural Icelandic glasses are dominated by S^{2-}, with $S^{6+}/\sum S$ <0.1. Experimental glasses are more oxidised, with $S^{6+}/\sum S$ between 0.51 and 0.87. This offers an opportunity to test whether oxidation state of sulfur influences the measured sulfur isotope ratio during SIMS analysis, which has not been previously investigated in detail.

4.2. Sulfur isotopic composition of glasses and observed IMF

Bulk sulfur isotope ratios measured by GS-IRMS in the glass samples are reported in Table 1. Four experimental glasses have $\delta^{34}S$ between 11.0‰ and 12.0‰, close to that of the anhydrite used to add the sulfur to the samples (11.1‰). Exceptions are phonolite glass LS-17985 (8.8‰), and nephelinite glass LS-17980 (9.4‰); both glasses have a lighter isotopic composition than the anhydrite. However, these glasses contained residual sulfur after initial melting of the rock powders in a 1 atm furnace (see supplementary spreadsheets for starting compositions), which is the likely cause of the difference in $\delta^{34}S$ compared to the doping anhydrite. Compositions of natural Icelandic glasses are similar to those determined for MORB (−1.3‰ Labidi et al., 2013), with average $\delta^{34}S$ between −0.4‰ and − 1.1‰. We also report $\Delta^{33}S$ and $\Delta^{36}S$ values from the nine glasses (Table 1.), however we do not utilise these for this study. As indicated by the close to 0 $\Delta^{33}S$ and $\Delta^{36}S$ values (Table 1), variations in isotope ratios follow mass-dependent fractionation for all nine glasses. The $\Delta^{36}S$ values of the experimental glasses likely have large uncertainties compared to the three natural glasses due to the small mass of the samples used for the bulk analyses.

During sulfur isotope ratio analysis by SIMS, each glass sample was analysed in a chain of five analyses to determine whether they are sufficiently homogeneous to be used as primary calibration standards. After excluding analyses with anomalous counts for either isotope (> 30% change in count rate or > 2 times internal precision compared to the previous analysis on the same glass) the remaining 602 glass analyses were averaged by session for each sample. The largest variability is observed for the rhyolitic LIP-17714 glass which has a 2σ standard deviation between 1.1‰ and 1.8‰ in the five sessions it was measured (Fig. 2B). This reproducibility is similar to the combined uncertainty of individual measurements, which is between 0.7‰ and 2.4‰ for LIP-17714 (Fig. 2A). In session 9, LS-17985 had a standard deviation of 2.8‰, indicating the presence of isotopic heterogeneity. In the other glasses, reproducibility during a session is between 0.3 and 1.4‰ (Figs. 2B, 4), either smaller than, or similar to the internal precision (Fig. 2A). The low variability of measured $\delta^{34}S$ indicates that at least eight of the nine glasses used in this study are suitable as SIMS primary standards, the exception being LS-17985, which may be less suitable as repeated EPMA (n = 7) and SIMS (n = 23) analyses from this sample produced variable measured sulfur contents and sulfur isotope ratios (see discussion for more detail).

Instrumental mass fractionation for sulfur isotope ratios can be expressed in ‰ using the following equation:

$$\mathrm{IMF}(‰) = \left(\left(^{34}S/^{32}S\right)_{\mathrm{drift}} - \left(^{34}S/^{32}S\right)_{\mathrm{bulk}}\right) \Big/ \left(^{34}S/^{32}S\right)_{\mathrm{bulk}} * 1000 \qquad (5)$$

where $(^{34}S/^{32}S)_{drift}$ is the drift-corrected sulfur isotope ratio and $(^{34}S/^{32}S)_{bulk}$ is the sulfur isotope ratio measured by an independent technique not affected by matrix effects. We find significant IMF (i.e. above internal and external analytical uncertainty) between glasses with different composition and sulfur content (Fig. 4). Compared to our primary drift standard EGT17–01 most glasses display a negative IMF, as large as −12‰ in the case of STAP. The only exception is TNR14–01, which has a positive IMF of +1‰ relative to EGT17–01. A significant variability in IMF can be observed between different sessions: HAW-16095 and LS-17980 have IMF between −2.5 to 1‰ and − 4.5 to −2‰, respectively (Fig. 4B). A significant difference can be observed between the IMF measured for LIP-17714 during session 1 and other sessions: IMF in session 1 is considerably smaller (−2‰) compared to other sessions (between −6‰ and − 8‰, Fig. 4). Natural Icelandic glasses all display a negative IMF, with the largest values observed for the sulfur-poor STAP glass, between −9.5 and − 12‰. Both LS-17980 (basanite) and LS-17985 (phonolite) have similar IMF, varying between −5‰ and − 2‰.

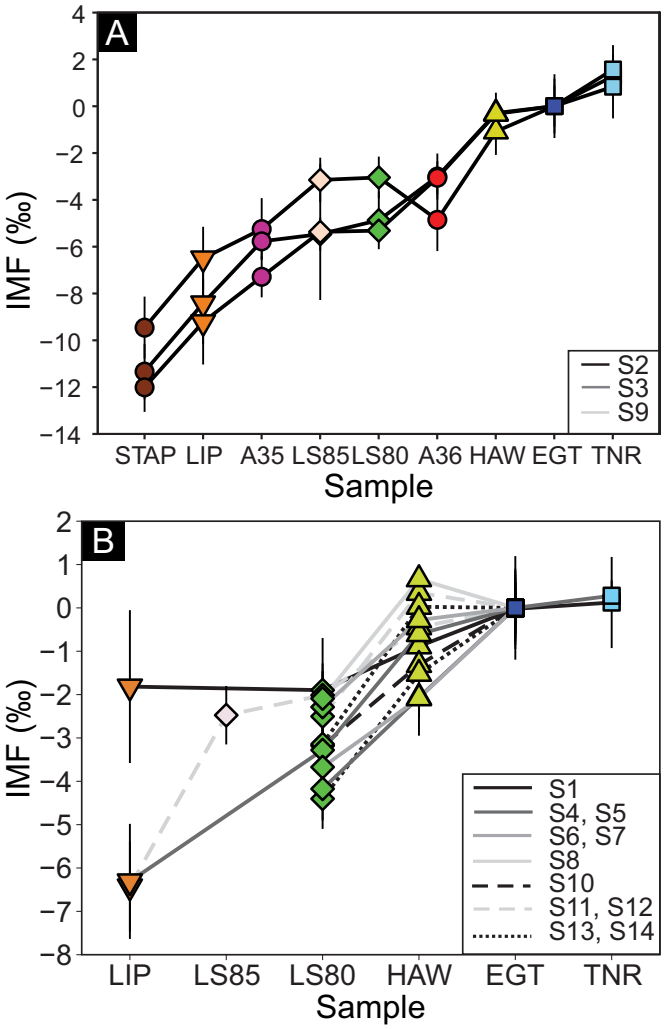

Fig. 4. Diagrams showing IMF values between different sessions, calculated relative to the primary drift standard EGT17–01, which is fixed at 0. In (A) sessions during which all nine glasses were measured are shown, while in (B) data from all other sessions are presented. Symbols are the same as in Figs. 1 and 2. Errors are 2σ standard deviation for each glass by session. EGT17–01, HAW-16095, and LS-17980 were measured in all 14 sessions. Note the difference in y-axis scale between (A) and (B).

5. Discussion

If a correlation exists between IMF measured in calibration standards and one or more chemical/physical parameters, IMF can be predicted and corrected for in materials with an unknown isotope composition. If IMF is controlled by the chemistry or the physical properties of the samples, such as density, a correlation should be observed between these

parameters and observed IMF (Deloule et al., 1991; Eiler et al., 1997; Hauri et al., 2006; Hartley et al., 2012). Instrumental mass fractionation can be calculated for *n* linear predictors as

$$\mathrm{IMF} = m_1{*}x_1 + m_2{*}x_2 + m_3{*}x_3 + \ldots + m_n{*}x_n + c \quad (6)$$

where m_1 to m_n are the slopes of the regression for each parameter, x_1 to x_n are the values of parameters 1 to n, and c is a constant. The number of predictors should be kept to a minimum, as their number is limited by the number of predicted values, in this case by the number of standards used to calculate IMF. In this discussion, we explore possible correction methods for composition-dependent IMF during sulfur isotope ratio analysis of glasses by SIMS using simple univariate linear, multivariate linear, and non-linear regression models.

5.1. Univariate linear models between glass composition and IMF

Univariate linear models are the simplest way to correct for composition-dependent IMF. For the purpose of statistical modelling, we used data collected during sessions 2, 3, and 9. In these sessions data were collected from all nine glass standards (Fig. 4A). When calculating regression for hydrogen, water contents measured by SIMS were used; this also applies to multivariate models discussed later. Results of univariate linear models are presented in Fig. 5. Linear regression modelling was carried out separately for all glass compositions (Fig. 5B) and for mafic glasses only (A35, A36, EGT17–01, HAW-16095, LS-17980, and TNR14–01, Fig. 5A). In both cases, the best correlation is between IMF and glass sulfur content (Fig. 5), which positively correlate with each other (Fig. 6). When all glass standards are used, R^2 between IMF and sulfur contents measured by SIMS are 0.79 to 0.90 (Fig. 5). A strong correlation can be observed when cps-based S contents are used (R^2 of 0.83 to 0.91), while R^2 is lower when EPMA S contents are used (0.71 to 0.81). If sulfur, measured by SIMS, is expressed as cations rather than by weight (ppm), R^2 is between 0.85 and 0.88. Other chemical and physical parameters have weaker correlations: after sulfur, the best correlation is observed between IMF and Fe^{3+} cations, which correlate positively and have R^2 values between 0.59 and 0.66. Similar results are obtained using only mafic glasses: sulfur correlates well with IMF. For mafic glasses IMF also correlates positively with $Fe^{3+}/\sum Fe$ and $S^{6+}/\sum S$ ratios and negatively with the molar volume of the glass (Fig. 5B), calculated using the method of Lange (1997). Nonetheless, R^2 values for these parameters are below 0.6 when all glasses are used (Fig. 5B).

Simple univariate regression models indicate that glass sulfur content might play a major role in controlling IMF during sulfur isotope ratio analysis by SIMS. Negative correlations between the H_2O content of glasses and IMF during D/H analyses by SIMS have been documented (Hauri et al., 2006; Befus et al., 2020); this correlation was attributed to changes in sputter rate and secondary ion yields of H and D with changing H_2O content. Hauri et al. (2006) used a two-step cascade model to explain IMF observed during their D/H analyses. After applying a kinetic energy transfer model together with a empirical regression using glass H, Si, and Fe contents to correct for the observed IMF, they were able to reproduce their bulk D/H values within 4σ analytical uncertainty. In session 3 we find a broad positive correlation between the S content of our glasses and ion yields of $^{32}S^-$ and $^{34}S^-$, with the exception of phonolitic glass LS-17985, which has an approximately 15–20% lower ion yield compared to other glasses with similar S content (Fig. 6A,B). A correlation between ion yield and S content may indicate that a similar process causes IMF during SIMS analyses of $^{34}S/^{32}S$ ratios as suggested during D/H analyses by Hauri et al. (2006). However, a correlation between ion yields and S content is not evident for sessions 2 or 9 in our dataset (see supplementary Fig. S4). We did not measure SIMS pit depth in the glasses, hence we cannot explore potential correlations between IMF and sputter rate, formation efficacy of S ions, or the Cs^+ concentration at the bottom of the crater floor (Eiler et al., 1997). Nonetheless, we can hypothesise that sputter rate is unlikely to strongly correlate with observed IMF. It would be expected that sputter rate is similar in glasses with similar major element compositions and physical properties such as density; for example, data presented by Hauri et al. (2006) shows a broad negative correlation between sputter rate and density. The three natural glasses from Iceland (A35, A36, and STAP) are similar in composition (Fig. 1), however they have different IMF, with STAP being extremely negative in all sessions it was analysed in. Further sputtering experiments could confirm whether secondary ion

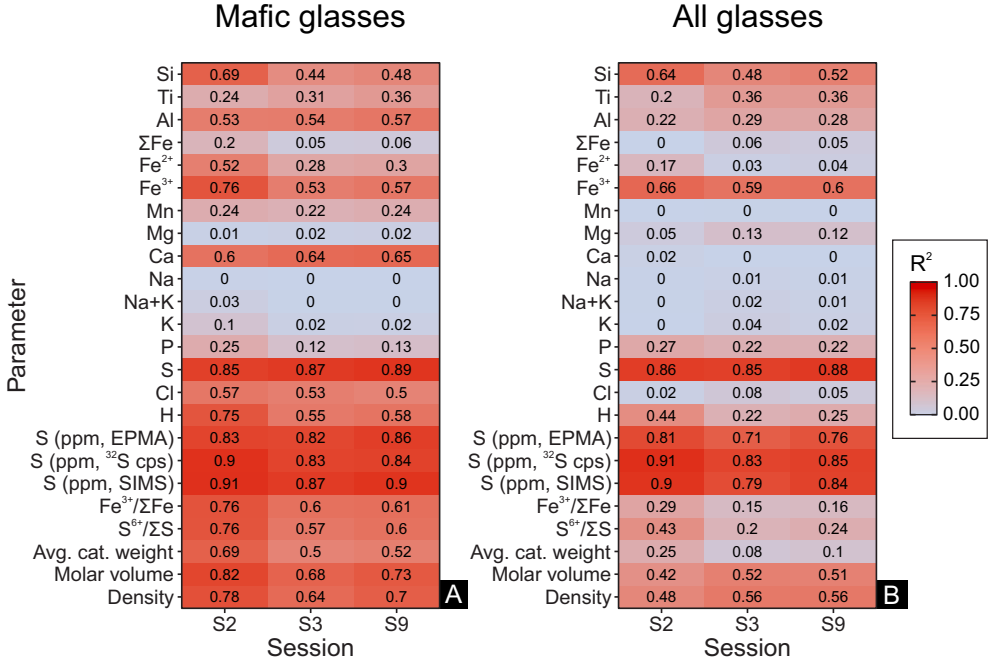

Fig. 5. R^2 values calculated using univariate linear regression models between R^2 and various parameters indicated along the y-axis for mafic glasses (A) and all glasses (B), using data collected during sessions 2, 3, and 9. During these sessions all nine glasses were analysed. Linear regression models are calculated using cation fractions of the glasses, normalised to 1. Molar volume (cm^3/mol) and density (g/cm^3) of the glasses are calculated using the method of Lange (1997).

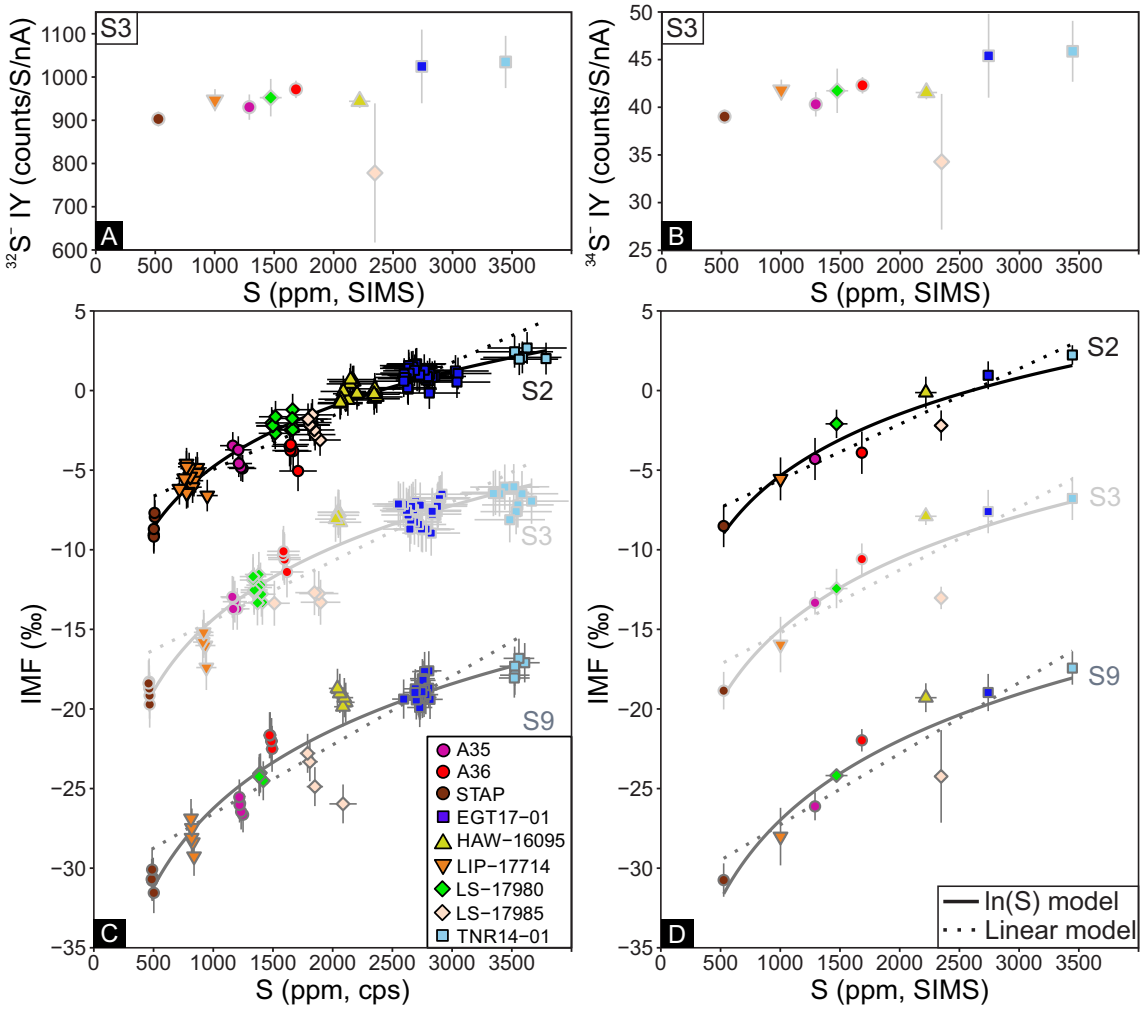

Fig. 6. Ion yields of $^{32}S^-$ (A) and $^{34}S^-$ (B) plotted against S content for session 3. Ion yields are expressed as counts (4 s cycle) / S (ppm) / nA primary current. Ion yields drop approximately 10% (from 1030 to 900) between our most S-rich glass and most S-poor glass in session 3, with the exception of phonolite LS-17985, which has a significantly lower ion yield (780) compared to the other 8 glasses. In (C) and (D) results of linear and logarithmic regression modelling between observed IMF, plotted un-normalised to EGT17–01, and S content are shown. The offset between the three curves is caused by EM ageing that resulted in the loss of $^{34}S^-$ counts over the two week analytical period. Data are from sessions 2, 3, and 9. In (C) sulfur contents are calculated from $^{32}S^-$ cps/nA, while in (D) S contents are measured by SIMS (see text for details). All errors are 2σ. Logarithmic fit to the data estimates IMF considerably better than linear models. The IMF of the phonolitic glass LS-17985 is not reproduced by either linear or logarithmic models accurately, likely due to its low ion yields. Data suggest ion yield of sulfur may be composition dependent, with less efficient ionisation observed in the extremely alkali- and aluminium-rich glass LS-17985.

yields from glasses, or the Cs concentration at the crater floor can explain, even if just partially, the observed IMF during S isotope ratio analyses of glasses by SIMS.

Previous studies have not observed IMF during sulfur isotope ratio analysis of glasses by SIMS; our results indicate this may be because only one standard material was used for calibration (Gurenko et al., 2001; Black et al., 2014; Beaudry et al., 2018). Studies of sulfur isotope ratios measured by SIMS using multiple glass standards are rare: Fiege et al. (2014) presented analyses of sulfur isotopes from 11 glasses, including basaltic, andesitic and rhyolitic compositions with known bulk sulfur isotope ratios, and found no evidence of composition-dependent IMF, albeit using glasses covering a smaller sulfur content range (521–1830 ppm) compared to those used for this study. Based on data presented in their paper and using our eq. 5, we calculate that six of the 11 glasses studied by Fiege et al. (2014) have larger IMF than their reported 2σ uncertainty of 0.52‰. IMF is up to 3.8‰ in their dataset. While Fiege et al. (2014) uses a linear regression between SIMS and bulk $\delta^{34}S$ data (which is close to unity with a constant instrumental bias of 1.84‰) to correct their data, no discussion is provided on the cause of the difference between SIMS and bulk $\delta^{34}S$ for some of their glasses, which is as high as 2.2‰ after correction for instrument bias. The analytical procedures used by Fiege et al. (2014) are different compared to those used in this work: their analyses were carried out in single-collector mode using two EM detectors. Different analytical conditions could be the cause of different observations regarding IMF during sulfur isotope ratio analysis in glasses. Shimizu et al. (2019) used two MORB glasses with close to identical composition as standards for their analyses, and no indication of composition-dependent IMF can be observed in their dataset. However, they experienced a large drift in measured sulfur isotope ratios over analytical sessions and a constant offset between bulk and SIMS sulfur isotope ratios, which we also observe in all of our sessions.

5.2. *Multivariate and non-linear models*

It is possible that IMF is not controlled by a single parameter, or by one parameter that is a combination of multiple independent variables (such as Na + K), but rather a combination of them, such that different parameters are required to explain observed variation in measured and true isotopic ratios (e.g Deloule et al., 1991; Vielzeuf et al., 2005;

Manzini et al., 2017). Non-linear correlations between IMF and various parameters also have been observed, such as for $\delta^{18}O$ analyses in olivines (Eiler et al., 1997), for $\delta^{18}O$ and $\delta^{13}C$ analyses in carbonates (Śliwiński et al., 2018), and for $\delta^{25}Mg$ analysis in olivines and pyroxenes (Fukuda et al., 2020).

We performed multivariate linear regression modelling using various combinations of elements, reported in Fig. 7. Elements were combined on the basis of their abundance, ionic charge, and to a smaller degree, their coordination in the glass (tetrahedral or octahedral). We also calculated a logarithmic regression between IMF and glass sulfur content (Fig. 6C,D) to explore whether a significant improvement can be achieved compared to linear fits. Similar to univariate models, multivariate regression modelling was carried out for data collected during sessions 2, 3 and 9.

Multivariate regression models were calculated on three different sample sets: mafic glasses (Fig. 7A,B), mafic glasses + rhyolite (including LIP-17714, but excluding phonolitic glass LS-17985, Fig. 7E, F), and all nine glasses including the phonolitic glass LS-17985 (Fig. 7C, D). Model calculations were also performed excluding phonolitic glass LS-17985 as we detected some heterogeneity in the measured sulfur contents between individual chips, indicated by the large error of EPMA-derived sulfur contents (~590 ppm 2σ uncertainty, Fig. 1B). Sulfur count rates and sulfur isotope ratios often varied significantly between and during SIMS analyses for LS-17985 (Fig. 2B).

The multivariate models combining alkalis, Al, and other elements such as Si and Ca show the largest R^2 values (Fig. 7). Univariate linear fits for Al, Na and K have R^2 <0.30 (Fig. 5B), while combining Al-Na-K in a trivariate regression model results in R^2 of 0.83 to 0.86 when all glasses are used (Fig. 7C). Adjusted R^2, calculated as

$$R^2_{adj} = 1 - \left(1 - R^2\right)*((n-1)/(n-p-1)) \quad (7)$$

where n is the number of observations and p is the number of predictors, which is an indicator of whether the addition of a new parameter into the model improves fits significantly, is 0.72 to 0.77 for the Al-Na-K model (Fig. 7D), a large improvement compared to univariate models. Other multivariate models such as Si combined with high abundance and mostly tetrahedrally coordinated cations (Al, Fe^{3+}, Ti), or combinations of 2+ charged octahedral cations do not improve fits significantly compared to univariate linear models, indicated by the decreasing adjusted R^2. Combining total Fe contents with sulfur improves R^2 but not R^2_{adj} when compared to the sulfur-only model, therefore improvement in the fit is minimal compared to the increase seen for the Al-Na-K model. Combining Al-Na-K with Si shows some improvement in R^2 and increases R^2_{adj} for data collected in session 2 when compared with the Al-Na-K model (Fig. 7).

If modelling is performed after excluding LS-17985 from the dataset, R^2 of the Al-Na-K model increases significantly to 0.87–0.996 (Fig. 7E), providing a better fit than the univariate regression between IMF and SIMS-based sulfur contents (including those derived from ^{32}S cps, Fig. 5B). Addition of Si into the model at this point does not significantly increase the quality of the fit, indicated by the lack of increase in adjusted R^2 values (Fig. 7F). The cause of the large increase in R^2 for the Al-Na-K model after excluding LS-17985 is due to the extremely high alkali (up to 18 wt% $Na_2O + K_2O$) and Al_2O_3 (>20 wt%) contents of the

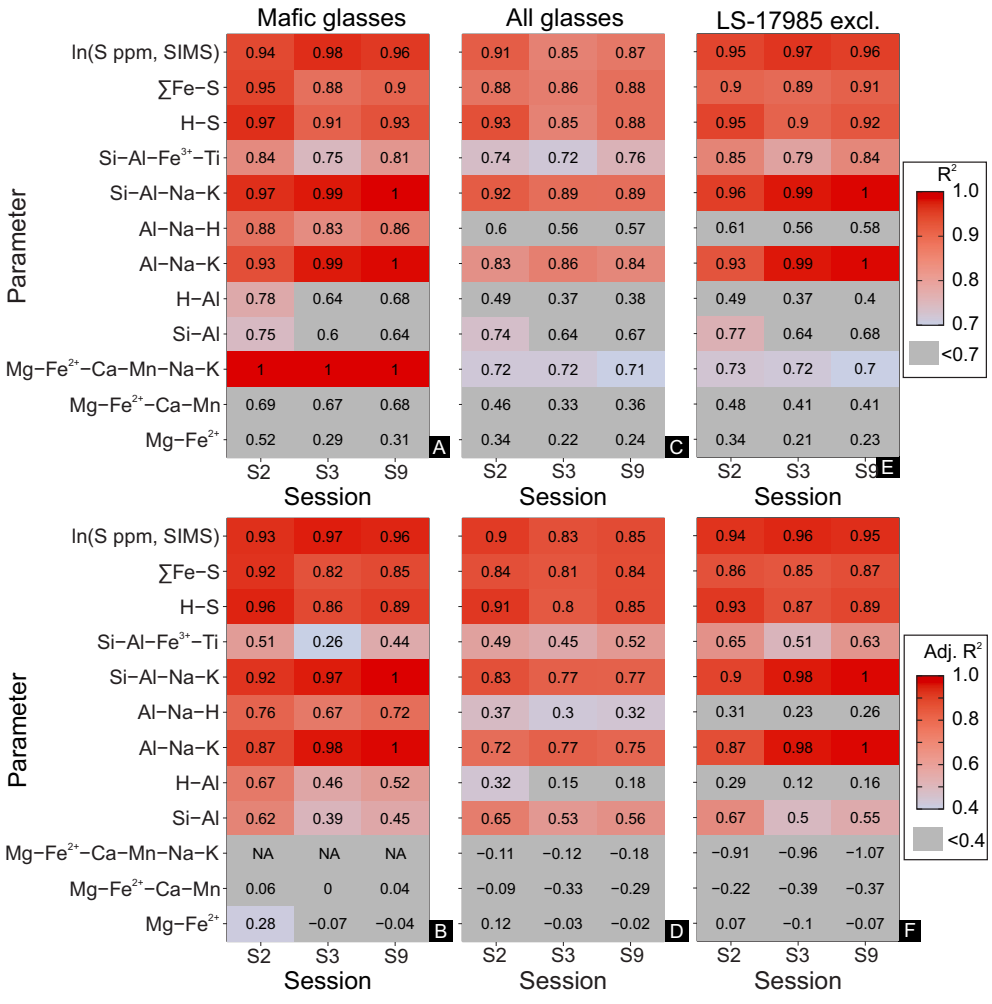

Fig. 7. Results (R^2 in A,C,E and adjusted R^2 in B,D,F) of non-linear and multivariate linear regression models using sulfur isotope data collected in sessions 2, 3, and 9. Calculations were performed using only mafic glasses (A-B), all glasses (C—D), and excluding LS-17985 (E-F). Note the colour scale difference between (A,C,E) and (B,D,F). In (B), NA indicates that adjusted R^2 for the Mg-Fe^{2+}-Ca-Mn-Na-K model is not applicable as the number of predictors is equal to the number of fitted values. For regressions that contain S as a parameter the SIMS-based S contents were used.

phonolithic LS-17985 glass. Due to this extremely high alkali and Al content LS-17985 will have the strongest leverage on the slopes of the Al-Na-K regression model.

A logarithmic fit between IMF and glass sulfur content provides a better fit than the linear models (Fig. 6). Logarithmic fits between IMF and SIMS glass sulfur contents have R^2 between 0.85 and 0.91 when all glasses are included in the fit, while R^2 is between 0.95 and 0.97 if LS-17985 is excluded (Fig. 7, Table 2). Linear models fail to fit IMF values measured in STAP, A35, and TNR14–01, with absolute values of residuals often > 1‰ for these three glasses. However, residuals for STAP and TNR14–01 decrease to < 1‰ if a logarithmic model is applied. (Table 2).

Statistical models clearly show that IMF arising during sulfur isotope analysis in glasses by SIMS is best predicted by either multivariate linear regression (Al-Na-K) or non-linear (ln(S)) regression models. Instrumental mass fractionation during sulfur isotope analysis of glasses by SIMS is best predicted by either a logarithmic fit to the sulfur content of the glasses or by a multivariate model using glass Al, Na, and K contents.

5.3. Predicting instrumental mass fractionation using glass chemistry

To test which elements can be used to predict IMF within analytical uncertainty, the $\delta^{34}S$ values of the analysed glasses were recalculated using modelled IMF values and compared with glass $\delta^{34}S$ measured by GS-IRMS. As at least three different standard glasses were analysed in every session, models using one or two predictors can be applied to data collected in all of the 14 sessions (602 analyses in total). Models with more than two predictors can only be calculated for certain sessions (Table 3). If all nine glasses are used during model calculations, the best performing model is a logarithmic fit to the SIMS-derived sulfur contents (ln(S, SIMS)): 46% and 79% of analysis are reproduced within 1σ and 2σ combined analytical uncertainty, respectively. Two regressions combining either glass S and H contents or total Fe and S contents also reproduce the bulk $\delta^{34}S$ to a similar accuracy (Table 3.). Both the H—S and ΣFe-S models perform > 5% better than the S-only linear model. Other models only reproduce < 75% of measurements within 2σ uncertainty, meaning more than 1 in 4 analyses will still be biased after the correction is applied (Table 3).

Glass LS-17985 is slightly heterogeneous and its high alkali and Al content has a large leverage on most regression. If this glass is excluded from the modelling procedure, both the logarithmic model using sulfur content measured by SIMS and the multivariate model based on glass Al-Na-K contents reproduce a larger number of standards within the 2σ analytical uncertainty. The Al-Na-K model reproduces 86.7% of the sulfur isotope ratios within 2σ uncertainty, while the ln(S, SIMS) model reproduces 83.9% (Table 3). Adding Si as a further parameter to the Al-Na-K model increases the accuracy of the IMF correction scheme, with 91% analyses reproduced within 2σ uncertainty, albeit this regression scheme can only be used for data collected in three sessions due to the larger number of predictors. These models could therefore serve as potential correction methods for composition-dependent IMF, as more than eight out of ten analyses will be unbiased within 2σ combined analytical uncertainty after applying these corrections. The ln(S, SIMS) model is preferred to the ln(S, EPMA) model; the difference between the two models likely reflects the inaccurate EPMA data acquired from glasses with mixed valence S. The Si-Al-Na-K model performs better than the Al-Na-K model when LS-17985 is included in the dataset, but the difference becomes relatively smaller (< 5%) once LS-17895 is excluded (Table 3); either regressions could be used to correct for IMF with a similar level of accuracy. We note that, due to the transitive nature of linear regressions, the variable ln(S, SIMS) also correlates with glass Al-Na-K contents; however this is not proof of a causal relationship between the two variables and observed IMF.

While a logaritmic regression model using cps-based glass S contents also provides good results in terms of reproducing the real $\delta^{34}S$ of our glass standard (80% if all nine glasses are included), its value is derived from the same analyses as the sulfur isotope ratios as it is based on the ^{32}S count rate. Therefore it cannot serve as a fully independent correction method for composition-dependent IMF during sulfur isotope analysis. The Al-Na-K model, after the exclusion of phonolitic glass LS-17985 from the dataset, reproduces standard compositions slightly better than the ln(S, SIMS) model, and is completely independent of the SIMS analysis as glass Al, Na and K contents derive from EPMA analyses. Even with the phonolitic glass excluded the Al-Na-K model is able to reproduce IMF for a large range of chemical compositions, including alkali-rich and alkali-poor mafic volcanics, and a rhyolite. The phonolitic glass LS-17985 exerts a disproportionately large control over the correlation for this model due to its alkali- and Al-rich composition (Fig. 1), hence this one glass can skew predicted IMF for other standards. Furthermore, LS-17985 displays some signs of inter-fragment heterogeneity as seen in data from session 9 (Fig. 8C, F), which justifies its exclusion. However, it might still be appropriate as a matrix-matched standard for evolved alkali volcanic glasses.

5.4. Possible causes and implications of IMF during sulfur isotope analyses in glasses by SIMS

Processes controlling secondary ion formation during sample bombardment are not well understood, and cannot be predicted using current physical models (Hinton, 1995). Therefore no process can be clearly implicated as the cause of the observed composition-dependent IMF. During oxygen and hydrogen isotope analyses by SIMS, IMF may occur due to collision-cascades between secondary ions, as this process preferentially transfers energy to heavy isotope species (Eiler et al., 1997; Hauri et al., 2006), and hence causes isotope fractionation. Generally, such models would be appropriate to explain correlations between IMF and elements that are abundant in most glasses, such as Si and Al, as these elements are the most likely to collide with secondary ions of the analyte. We find indication that the secondary ion yield of sulfur in glasses may be composition-dependent. In session 3 a broad decrease in ion yields can be observed in glasses with low S content for both isotope species (Fig. 6A,B); however, this correlation is not evident in sessions 2 and 9 (Fig. S4). In most sessions the lowest ion yields are measured for phonolitic glass LS-17985; this glass has extremely high Al, Na, and K contents compared to all our glasses, which suggest a link exists between S ion yields and glass composition. More crucially, this may provide a link between IMF correlating with S content and glass Al-Na-K content simultaneously.

The relationship observed between IMF and glass S content could be explained by a number of analytical artefacts. These include incorrect deadtime correction on the EM detector measuring $^{34}S^-$ ions, a minor overlap between the $^{32}S^-$ peak (mass 31.9721) and the $^{16}O_2^-$ peak (mass 31.9898), fluctuations of the baseline on the FC detector measuring $^{32}S^-$, or non-linear detector response. As size of the deadtime is count rate dependent for $^{34}S^-$ (eq. 2), and count rate is itself dependent on S content, incorrectly estimating deadtime could cause an analytical artefact resulting in a positive correlation between S content and IMF. We measured an IMF of < -10‰ on STAP, which can only be explained if we underestimated by ~50 ns (see supplementary material for more detail). The error of our measured deadtime estimate is < 1 ns, hence we can exclude incorrect EM deadtime as a possible explanation for the correlation between IMF and S.

An overlap between the $^{32}S^-$ and $^{16}O_2^-$ peaks could cause a correlation between S content and IMF. As seen from the mass scans (Fig. 3), the effective mass resolution of our analytical setup is ~2060 on the FC detector, and the two peaks are not fully resolved. All our glasses have similar O contents (43.9–54.0 wt%), meaning all the 9 glasses will have $^{16}O_2^-$ peaks of similar intensity; however the size of the $^{32}S^-$ peak is variable, as the relative S range in the glasses is large (0.05 to 0.34 wt%, a seven times increase). A peak overlap would cause elevated $^{32}S^-$ counts compared to $^{34}S^-$, with S-poor glasses being the most affected, resulting in a decrease in $^{34}S/^{32}S$ with decreasing S content. To test

Table 2
Results of selected regression models, including residuals, R^2 and adjusted R^2 values. These models provide the best fits for sulfur isotope data collected during sessions 2, 3, and 9.

Parameter	Session	LS-17985 Included	Residuals									R^2	Adjusted R^2
			A35	A36	EGT17-01	HAW-16095	LIP-17714	LS-17980	LS-17985	STAP	TNR14-01		
S (SIMS)	S2	Included	0.3	-0.7	0.5	1.2	0.0	1.9	-1.3	-1.3	-0.7	0.90	0.88
S (SIMS)	S3	Included	0.7	1.9	0.7	2.5	-0.7	0.9	-3.1	-1.8	-1.2	0.79	0.77
S (SIMS)	S9	Included	-0.1	2.3	0.5	2.5	-0.8	1.0	-3.0	-1.4	-1.1	0.84	0.82
S (SIMS)	S2	Not included	0.2	-0.8	0.2	1.0	0.0	1.7	NA	-1.3	-1.0	0.92	0.90
S (SIMS)	S3	Not included	0.5	1.6	0.1	2.0	-0.9	0.6	NA	-1.8	-2.0	0.88	0.86
S (SIMS)	S9	Not included	-0.4	1.9	-0.1	2.1	-0.9	0.7	NA	-1.4	-1.9	0.91	0.89
ln(S, SIMS)	S2	Included	-0.4	-1.5	0.7	0.8	-0.2	1.1	-1.6	0.5	0.7	0.91	0.90
ln(S, SIMS)	S3	Included	0.0	1.0	0.9	1.9	-1.0	0.1	-3.6	0.3	0.2	0.85	0.83
ln(S, SIMS)	S9	Included	-1.0	1.3	0.7	1.9	-1.1	0.0	-3.4	0.9	0.6	0.87	0.85
ln(S, SIMS)	S2	Not included	-0.5	-1.7	0.3	0.5	-0.3	0.9	NA	0.5	0.2	0.95	0.94
ln(S, SIMS)	S3	Not included	-0.3	0.6	0.1	1.3	-1.1	-0.3	NA	0.5	-0.7	0.97	0.96
ln(S, SIMS)	S9	Not included	-1.3	0.8	0.0	1.3	-1.2	-0.4	NA	1.0	-0.2	0.96	0.95
ΣFe-S	S2	Included	-0.1	-1.2	0.4	1.6	-0.3	2.2	-1.2	-0.9	-0.5	0.88	0.84
ΣFe-S	S3	Included	-0.5	0.1	0.6	2.9	0.5	1.2	-1.6	-1.7	-1.5	0.86	0.81
ΣFe-S	S9	Included	-1.4	0.4	0.4	2.9	0.4	1.3	-1.5	-1.3	-1.3	0.88	0.84
ΣFe-S	S2	Not included	0.1	-0.9	0.0	1.3	-1.0	2.0	NA	-0.7	-0.8	0.90	0.86
ΣFe-S	S3	Not included	-0.2	0.5	0.1	2.5	-0.5	1.1	NA	-1.5	-1.9	0.89	0.85
ΣFe-S	S9	Not included	-1.2	0.8	-0.1	2.6	-0.6	1.2	NA	-1.1	-1.6	0.91	0.87
H-S	S2	Included	0.8	-0.5	0.4	1.0	-0.9	1.3	-1.1	-0.5	-0.5	0.93	0.91
H-S	S3	Included	0.3	1.0	0.5	2.7	-0.5	1.1	-2.4	-1.2	-1.4	0.85	0.80
H-S	S9	Included	-0.5	1.4	0.3	2.7	-0.7	1.1	-2.3	-0.8	-1.2	0.88	0.85
H-S	S2	Not included	0.8	-0.5	0.2	0.7	-1.1	1.1	NA	-0.5	-0.7	0.95	0.93
H-S	S3	Not included	0.3	1.0	0.0	2.2	-1.0	0.6	NA	-1.2	-1.9	0.90	0.87
H-S	S9	Not included	-0.5	1.4	-0.2	2.2	-1.1	0.6	NA	-0.7	-1.7	0.92	0.89
Si-Al-Fe^{3+}-Ti	S2	Included	0.8	0.3	2.3	-0.9	1.1	-1.2	0.9	-3.6	0.3	0.74	0.49
Si-Al-Fe^{3+}-Ti	S3	Included	1.1	1.2	2.8	0.2	0.8	-1.2	0.9	-4.7	-1.1	0.72	0.45
Si-Al-Fe^{3+}-Ti	S9	Included	0.3	1.4	2.9	-0.2	1.1	-1.1	1.1	-4.7	-0.9	0.76	0.52
Si-Al-Fe^{3+}-Ti	S2	Not included	1.1	-0.6	2.7	0.3	0.2	-1.5	NA	-1.5	-0.6	0.85	0.65
Si-Al-Fe^{3+}-Ti	S3	Not included	1.4	0.2	3.1	1.4	-0.1	-1.4	NA	-2.6	-2.0	0.79	0.51
Si-Al-Fe^{3+}-Ti	S9	Not included	0.7	0.3	3.3	1.3	0.1	-1.4	NA	-2.4	-2.0	0.84	0.63
Al-Na-K	S2	Included	1.0	-1.9	0.0	1.0	-2.1	-1.2	1.5	0.1	1.5	0.83	0.72
Al-Na-K	S3	Included	0.9	-0.3	-0.5	1.9	-2.1	-2.2	2.0	-0.5	0.8	0.86	0.77
Al-Na-K	S9	Included	0.1	0.0	-0.6	1.9	-2.6	-2.6	2.4	0.0	1.4	0.84	0.75
Al-Na-K	S2	Not included	0.9	-2.1	0.5	-0.1	-0.6	0.4	NA	0.3	0.7	0.93	0.87
Al-Na-K	S3	Not included	0.7	-0.6	0.3	0.3	0.0	-0.1	NA	-0.3	-0.2	0.99	0.98
Al-Na-K	S9	Not included	-0.1	-0.4	0.3	0.0	-0.1	-0.1	NA	0.2	0.1	1.00	1.00
Al-Na-H	S2	Included	1.2	-1.1	2.9	0.8	-4.5	-0.7	0.2	-0.5	1.7	0.60	0.37
Al-Na-H	S3	Included	0.8	-0.4	4.2	2.0	-5.6	-1.5	0.3	-0.7	0.9	0.56	0.30
Al-Na-H	S9	Included	0.0	-0.1	4.3	2.0	-6.2	-1.8	0.5	-0.2	1.4	0.57	0.32
Al-Na-H	S2	Not included	1.2	-1.1	3.1	0.7	-4.5	-0.5	NA	-0.5	1.6	0.61	0.31
Al-Na-H	S3	Not included	0.8	-0.4	4.5	1.8	-5.5	-1.2	NA	-0.7	0.8	0.56	0.23
Al-Na-H	S9	Not included	0.0	-0.1	4.8	1.7	-6.1	-1.3	NA	-0.3	1.2	0.58	0.26
Al-Na-K-Ca	S2	Included	0.9	-1.5	0.5	1.3	-1.6	-1.9	1.5	0.0	1.0	0.84	0.68
Al-Na-K-Ca	S3	Included	0.9	-0.3	-0.6	1.8	-2.2	-2.1	2.0	-0.5	0.9	0.86	0.71
Al-Na-K-Ca	S9	Included	0.1	0.0	-0.6	1.9	-2.6	-2.6	2.4	0.0	1.3	0.84	0.69
Al-Na-K-Ca	S2	Not included	0.8	-1.8	1.0	0.1	-0.1	-0.4	NA	0.1	0.2	0.94	0.87
Al-Na-K-Ca	S3	Not included	0.7	-0.6	0.2	0.2	0.0	0.0	NA	-0.3	-0.2	0.99	0.98
Al-Na-K-Ca	S9	Not included	-0.1	-0.4	0.3	0.0	-0.1	-0.1	NA	0.2	0.1	1.00	1.00
Si-Al-Na-K	S2	Included	1.4	-0.6	0.4	0.2	-0.2	-1.9	0.8	-0.7	0.7	0.92	0.83
Si-Al-Na-K	S3	Included	1.1	0.6	-0.3	1.3	-0.8	-2.7	1.6	-1.0	0.3	0.89	0.77
Si-Al-Na-K	S9	Included	0.4	1.1	-0.3	1.2	-0.9	-3.2	1.8	-0.7	0.6	0.89	0.77
Si-Al-Na-K	S2	Not included	1.1	-1.3	0.6	-0.3	0.2	-0.5	NA	-0.3	0.4	0.96	0.90
Si-Al-Na-K	S3	Not included	0.7	-0.6	0.3	0.3	0.0	-0.1	NA	-0.3	-0.3	0.99	0.98
Si-Al-Na-K	S9	Not included	-0.1	-0.2	0.3	0.0	0.1	-0.2	NA	0.1	0.0	1.00	1.00

Table 3
Results of IMF modelling using different correction methods. Glass $\delta^{34}S$ values are considered to be reproduced if after applying the IMF correction the resulting $\delta^{34}S$ is within the interval defined by the bulk $\delta^{34}S \pm 1\sigma$ and 2σ combined external uncertainty calculated using eq. 3.

Model	Sessions	n	LS-17985	Reproduced (%)	
				1σ	2σ
S, SIMS (linear)	All	602	Included	42.2%	71.8%
S, SIMS (linear)	All	579	Excluded	42.0%	74.3%
ln(S, EPMA)	All	602	Included	35.0%	62.5%
ln(S, EPMA)	All	579	Excluded	45.4%	73.9%
ln(S, SIMS)	All	602	Included	45.7%	78.9%
ln(S, SIMS)	All	579	Excluded	48.4%	83.9%
ΣFe-S	All	602	Included	52.3%	80.6%
ΣFe-S	All	579	Excluded	51.6%	82.0%
H-S	All	602	Included	51.5%	79.2%
H-S	All	579	Excluded	49.4%	81.0%
Al-Na-K	S1, S2, S3, S4, S9, S11	385	Included	36.9%	60.0%
Al-Na-K	S1, S2, S3, S4, S9	332	Excluded	57.5%	86.7%
Si-Al-Na-K	S2,S3,S9	242	Included	42.6%	73.1%
Si-Al-Na-K	S2,S3,S9	224	Excluded	53.6%	91.1%

whether this potential peak overlap is the cause of the observed correlation between IMF and S content, we carried out analyses on a number of our glasses at 2400 and 4800 mass resolution (see supplementary Fig. S6). If the correlation is caused by an overlap, IMF would become more negative for S-poor glasses at low mass resolution, and less negative at higher mass resolution. We observe no such relationship in data collected from the glasses at different mass resolutions (Fig. S6); Therefore, we can rule out an overlap as the cause of the IMF-S correlation.

A drift in the FC baseline (Fig. 3) could also cause a correlation between IMF and S content: the $^{32}S^-$ count rate on S-poor glasses is smaller, and would be more sensitive to the size of the FC baseline. We hypothesise that the FC baseline is unlikely to change more than the 10% over an analytical session that would be needed to cause up to −12‰ IMF on the most S-poor glass STAP. The current amplifier of the Cameca IMS-1270 FC-L1 detector is in a temperature controlled environment, therefore no FC baseline drift is expected due to changes in current amplifier temperature. The FC baseline noise (i.e. the standard deviation of the baseline) is close to 4000 counts (1σ, see supplementary material for more detail), so most variation in FC baseline may be simply due to thermal noise. We can also rule out non-linear detector response

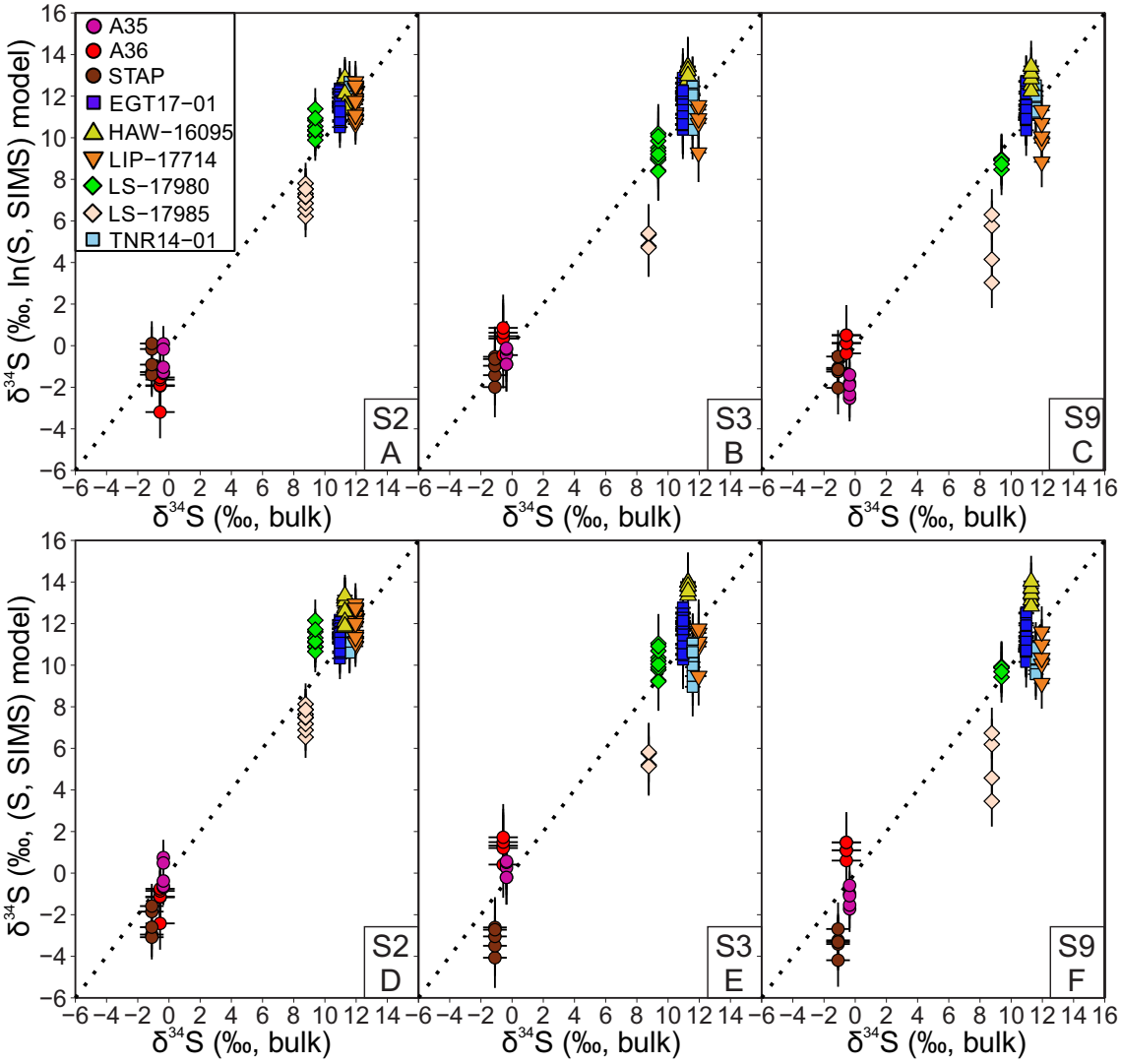

Fig. 8. Fitted $\delta^{34}S$ values corrected for IMF using the linear S and ln(S) models plotted against bulk $\delta^{34}S$ of the glasses. IMF is calculated using SIMS sulfur contents (oxygen RIY). A logarithmic regression is used in (A-C), while a linear regression is used in (D—F). The dotted lines show a 1:1 relationship. Each graph shows results for a different session (sessions 2, 3, and 9). Logarithmic models reproduce 37% and 67% of the bulk $\delta^{34}S$ values within 2σ combined external uncertainty for data collected during sessions 2, 3, and 9, respectively. Error bars are 2σ uncertainty on both axes.

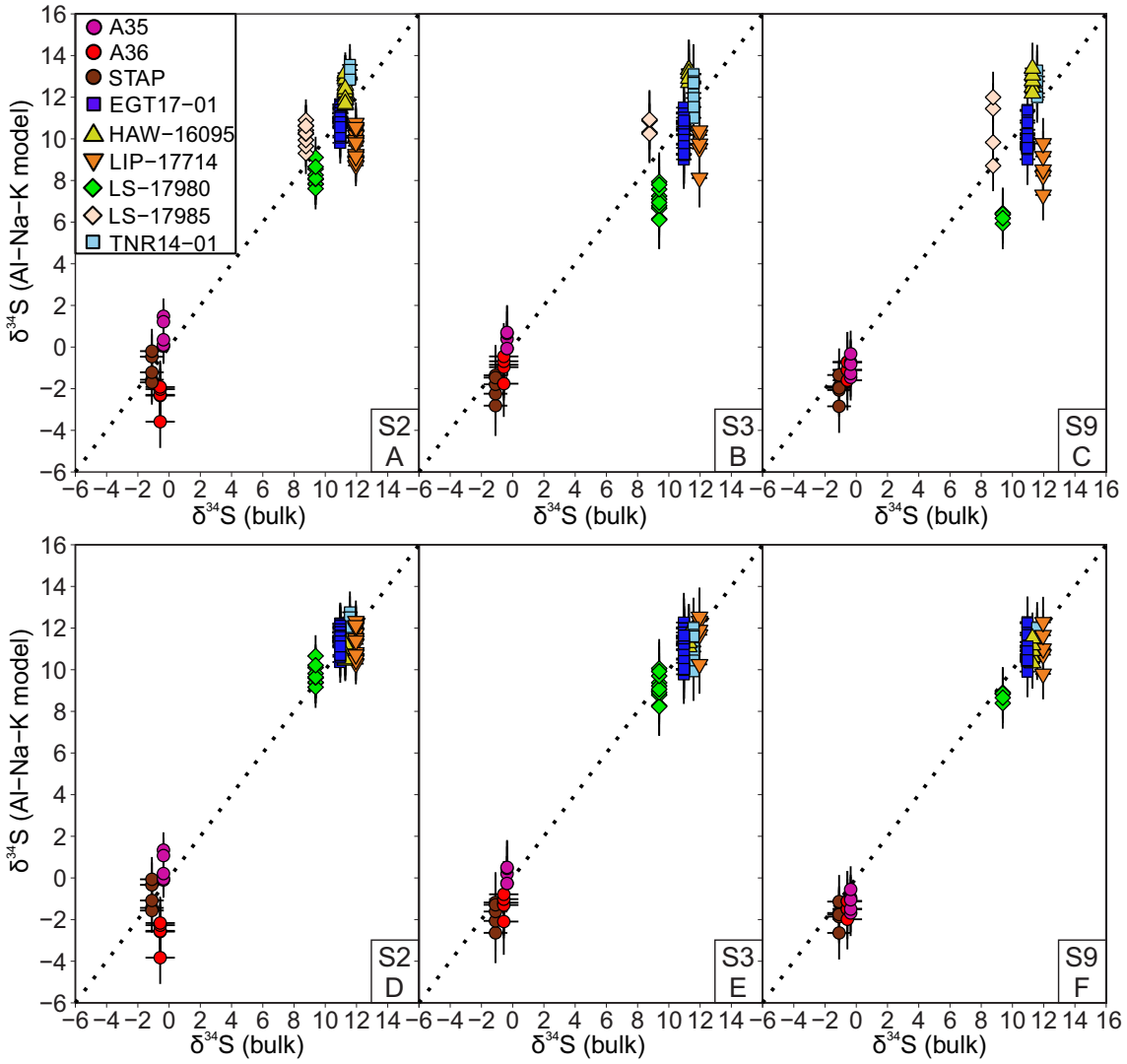

Fig. 9. Fitted $\delta^{34}S$ values corrected for IMF using the Al-Na-K multivariate regression model plotted against glass bulk $\delta^{34}S$. The dotted lines represent 1:1 relationship and session are the same as in Fig. 7. The top three graphs (A-C) show results using all glass analyses from the three sessions, while in the lower three graphs (D—F) LS-17985 was excluded. Using all glasses (A-C) 33% and 55% of the bulk $\delta^{34}S$ values are reproduced within 1σ and 2σ external uncertainty for the three session presented in this graph, respectively. The percentage of reproduced glass compositions increases to 58% (1σ) and 87% (2σ) when LS-17985 is excluded from the dataset.

as the cause of the IMF-S correlation, as $^{32}S^-$ and $^{34}S^-$ count rate correlate linearly, with an R^2 of 0.999 or better in every session (Fig. 10B, also see supplementary data).

Sulfur, Al, and alkali contents of the standard glasses could provide an explanation of what processes cause composition-dependent IMF in our dataset. Two glasses with the lowest observed IMF (HAW-16095 and TNR14–01, Fig. 4) relative to our primary drift correction standard EGT17–01 have the highest glass sulfur contents and lowest Al contents relative to their total alkali content (Figs. 1, 10). Natural Icelandic glasses have similar low alkali contents, but somewhat higher Al contents and lower sulfur-to-alkali ratios. However, natural Icelandic glasses have IMF between −3‰ to −12‰ (Fig. 4). Glass LS-17980, which is compositionally very similar to EGT17–01, has an average negative IMF of −3‰, with the only main difference between the two glasses being the sulfur content (Fig. 1B) and sulfur-to-alkali ratio (Figure 10:A). While this points to some degree of connection between IMF and sulfur-to-alkali ratios in the studied glasses, the correlation is not clear: EGT17–01 has a considerably lower S/(Na + K) ratio than HAW-16095, yet the latter sample has a negative IMF. Nonetheless, some relationship exists between IMF and S/(Na + K) at least for glasses with similar total alkali contents, such as the three Icelandic glasses (Fig. 10A).

Alkalis, such as Na and K, form 1+ ions and are highly reactive. During sulfur isotope analyses, secondary ions are analysed as $^{32}S^-$ and $^{34}S^-$, hence it is possible that negative sulfur ions interact with positively charged alkalis as the sample is ionised by the primary beam, producing complexes such as NaS^- and KS^-. Mass scans on the EM detector indicate a peak adjacent to the $^{34}S^-$ peak at mass ~33.890, corresponding to $H^{33}S^-$ (supplementary Fig. S5). For HAW-16095, the $H^{33}S^-$ count rate is 0.1% of the $^{34}S^-$ count rate (supplementary Fig. S5). Isotope ^{33}S is around six times less abundant than ^{34}S, which could indicate complex formation between 1+ charged ions like H^+, Na^+, and K^+ and sulfur ions, both 1- and 2- charged, may be an effective process. Mass spectra suggest one $H^{33}S^-$ ion forms for every 170 $^{33}S^-$ ion in HAW-16095, which decreases to one in 490 for STAP. As the electronegativity difference between alkalis and sulfur is relatively large (1.65 between S and Na, 1.76 between S and K) these bonds would be strongly ionic. If NaS and KS molecules form during beam-sample interaction they should preferentially incorporate heavier ^{34}S, as more complex, ionic bonded material favours the heavier isotopic species (Schauble, 2004). This

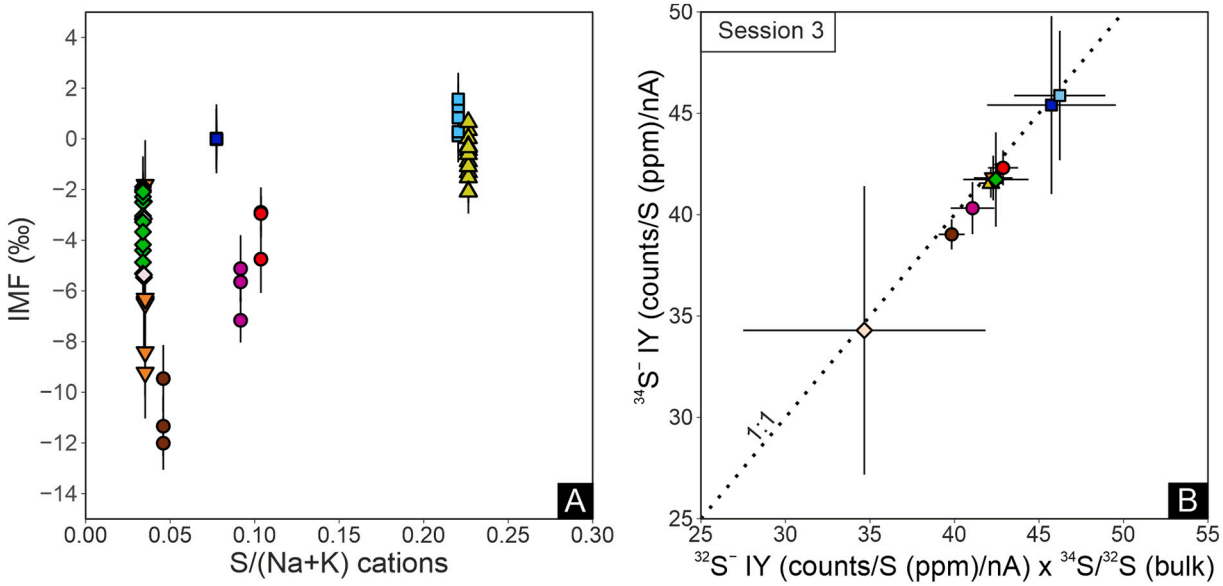

Fig. 10. Instrumental mass fractionation vs. atomic cation ratio of S/(Na + K) (A) and ion yields of $^{34}S^-$ per nA primary current vs. ion yield of $^{32}S^-$ per nA primary current in session 3 (B). Ion yields of $^{32}S^-$ were multiplied by bulk $^{34}S/^{32}S$ to scale isotope ion yields. In (A) each point represents an average value for IMF for each session in each glass. Error bars are 2σ. In (A) the amount of sulfur available to react with alkali elements (Na + K) during secondary ionisation relative to the alkali content of the glasses is shown. Glasses with similar Na + K content (see Fig. 1A), such as TNR14–01, HAW-16095, and the Icelandic glasses, have more negative IMF as their S/(Na + K) ratio decreases, indicating that interaction between alkalis and sulfur might be limited by the amount of sulfur present in the ionised sample material. In (B) a strong linear relationship between the ion yields of two isotopes show that detectors provide a strong linear signal, and that ion yield of alkali and Al-rich glass LS-17985 has a lower S ion yield than other glasses. Symbols are the same as in Fig. 9.

would result in the loss of $^{34}S^-$ ions relative to $^{32}S^-$ that reach the detector, causing a decrease in measured $\delta^{34}S$. If $^{34}S^-$ is lost disproportionately during ion beam-sample interaction to alkali elements, that could serve as a possible explanation for the correlation between the Al-Na-K regression model and observed IMF, albeit this process would likely require very effective isotope fractionation to be a feasible explanation.

A further consideration relates to caesium that becomes concentrated at the crater floor during primary Cs^+ beam bombardment. The concentration of Cs at the crater floor can be calculated from sputter yield (Eiler et al., 1997). We did not measure sputter yield from our glasses, although such data may provide further insight into the physical causes of IMF during S isotope analyses. Measurements carried out using Na^+ and K^+ primary beams on pure silicon show that these elements are effectively implanted into the sample surface due to their comparatively low sputter yields (Lareau and Williams, 1985). Therefore, it may be possible that Na and K content at the crater floor are elevated, hence these elements could influence S ion yields and cause subsequent isotope fractionation. Sodium and K would be further concentrated at the crater due to their low ion yields under a Cs^+ beam (Ireland, 2004), meaning small amounts of alkalis are extracted from the sample surface. For D/H isotopes, Hauri et al. (2006) suggested cascade collisions between secondary ions of H and D with other secondary ions resulted in isotope fractionation. This also offers a possible explanation for the observed IMF, although IMF generally does not correlate well with high abundance matrix elements like Si in our dataset (Figs. 5 and 7). Alkali elements are unlikely to form secondary ions during Cs^+ bombardment due to their low negative secondary ion yields, meaning S ions would be unlikely to collide with them during cascade collisions, so this process is not a feasible option to explain the IMF and Al-Na-K correlation.

A possible test for the hypothetical complex formation model is the measurement of KS^- and NaS^- count rates, ideally alongside $^{34}S/^{32}S$ within glasses, which would reveal any correlation between IMF and alkali-sulfur complex formation during sample beam interaction. However such measurements would be difficult to carry out in multi-collection mode due to the large mass difference between sulfur (masses 32 and 34), NaS (masses 55 and 57), and KS (masses 71 and 73) ions. Further work is required to better identify the causes of composition-dependent IMF, possibly using a larger set of felsic glass standards, with highly variable Al and alkali contents, to investigate possible interactions between Al, alkalis, and sulfur during sample-beam interaction. Measurement of sputter rate, and subsequent calculation of S ion sputter yields, ionisation efficiency, and Cs concentration at the bottom of the crater floor are further possible tests that may help identify the cause of IMF during S isotope ratio analyses of glasses by SIMS.

The correlation between IMF and glass Al-Na-K contents could have important consequences for sulfur isotope analysis of glasses and crystal-hosted melt inclusions from silica-rich volcanic systems, such as I- and S-type granites, rhyolites, and dacites, which cover a wider range of Al and alkali contents compared to most mafic magmas. Evolved alkaline magmas, such as trachytes and phonolites, would be affected by even larger IMF. Magmatic ore deposits are frequently linked to intrusions of I- and S-type granites, and hence their sulfur isotopic compositions may be of interest; however, the effects of IMF and the use of appropriate standards must be further considered if the sulfur isotopic compositions of silica-rich melts are to be studied by SIMS.

5.4.1. *Session-by session variation in measured glass sulfur isotope ratios*

Multivariate regression models, such as the Al-Na-K correction scheme, require the number of measured standards to be greater than the number of predictors (i.e. elements used in the fitting). This would require a large number of standards to be measured during each session. It is therefore important that the composition-dependent part of the IMF can be robustly predicted from one session to another, even after measuring just a few standards. Apart from IMF dependent on glass composition, the absolute value of measured sulfur isotope ratio by SIMS will be influenced by other factors such as detector sensitivity, EM ageing, and changes in primary and secondary ion beam conditions. This composition-independent IMF should produce a constant offset in measured sulfur isotope ratios, evident from the near-parallel fits between glass sulfur content and IMF for session 2, 3, and 9 (Fig. 6).

Instrumental mass fractionation calculated using both the Al-Na-K multivariate regression model and the logarithmic fit to glass sulfur contents produces near-parallel fits when compared to measured IMF (supplementary Fig. S3). This indicates that these correction schemes provide a reliable way to predict the composition-dependent component of the total IMF between different sessions; a few standards analysed regularly in each session are sufficient to obtain a good estimate for the constant offset in IMF that is composition-independent, i.e. instrument related. The calibration for composition-dependent IMF should be ideally carried out before the analysis of unknown samples. Composition-dependent IMF in our dataset stays constant for a relatively long (up to two weeks) time. As the multi-collector procedure used in this work only requires a short (< 4 min long) analysis time per measurement this approach enables the acquisition of large datasets in a relatively short time frame.

6. Conclusions

Sulfur isotope analyses of nine glass standards by multi-collector SIMS reveal significant composition-dependent instrumental mass fractionation effects in measured sulfur isotope ratios. The magnitude of the IMF is up to −12‰ in some glasses, and is greater than the analytical uncertainty of 0.7–2‰ (2σ) even at low sulfur contents (< 600 ppm). This result contrasts with previous studies where composition-dependent IMF during sulfur isotope ratio analyses was shown or assumed to be negligible. Multiple glass standards with known isotopic ratios covering at least the compositional range of unknown samples are required to investigate and accurately correct for composition-dependent IMF during multi-collector SIMS analysis of sulfur isotope ratios in glasses. Standard deviations measured for each session are lower than external uncertainty for eight of our nine glasses, hence they are suitable as primary standards; the one exception is our phonolitic glass, which displays heterogeneity above analytical uncertainty in terms of both sulfur content and sulfur isotope composition. Low analytical errors associated with count rates of both isotope species and drift correction reveal that SIMS offers a feasible way of discriminating per mille level changes in sulfur isotope ratios at the resolution of tens of microns in silicate glasses.

Statistical analysis using univariate, non-linear, and linear multivariate regression models reveals that observed IMF correlates logarithmically with glass sulfur content. A strong correlation is also observed between IMF and a multivariate regression model comprised of Al, Na, and K as predictors. After exclusion of our least reproducible phonolitic glass standard from the dataset we find that the ln(S) and the Al-Na-K multivariate regression models reproduce the bulk sulfur isotope ratios of the glasses for 84% (486 out of 579, 14 sessions) and 87% (288 out of 332, five sessions) of analyses within 2σ combined external uncertainty, which is between 0.6‰ and 1.5‰ for our glasses. Overall the Al-Na-K and the Si-Al-Na-K regression models offer the best accuracy when correcting for composition-dependent IMF. The correlation between IMF and glass S content resembles previous observations during D/H analyses of glasses by SIMS. Instrumental mass fractionation during sulfur isotope ratio analysis of glasses could be caused by alkali element accumulation at the bottom of the crater floor during sputtering or the formation of complex ions between alkali elements and sulfur during sample-beam interaction. Our standard set is useful to characterise composition-dependent IMF during analysis of sulfur isotopes in glasses by SIMS regardless of the process that causes the isotopic bias, and can be used to predict IMF for a large range of mafic glass compositions, while also being applicable to certain silica-rich glasses such as alkali-rich rhyolites. Further work, possibly using a larger standard set, and including sputtering experiments, is recommended to better understand sulfur isotope fractionation during glass SIMS analyses.

Declaration of Competing Interest

The authors declare that they have no known competing financial interests or personal relationships that could have appeared to influence the work reported in this paper.

Acknowledgements

We thank Rick Hervig and an anonymous reviewer for their constructive and helpful reviews. This work was supported by NERC studentship NE/L002469/1 to Z.T. and NERC grants IMF688/0519 and NE/P002331/1 to M.E.H. D.A.N. was supported by the German Research Foundation (NE2097/1–1) and a Presidential Fellowship from the University of Manchester. S.A.H acknowledges support from the Icelandic Research Fund (Grant #196139-051). We thank Tamsin Mather (University of Oxford) for allowing us to use data collected from our glasses as part of the NSFGEO-NERC grant NE/T010940/1 and NERC grant IMF703/0520. We thank John Craven at the Edinburgh Ion Microprobe Facility (EIMF) for his assistance during the ion probe analyses, data processing, and interpretation, Jonathan Fellowes for the assistance with the electron microprobe measurements and Lewis Hughes for his help with the FTIR analysis in Manchester.

Appendix A. Supplementary data

Supplementary data to this article can be found online at https://doi.org/10.1016/j.chemgeo.2021.120318.

References

Beaudry, P., Longpré, M.-A., Economos, R., Wing, B.A., Bui, T.H., Stix, J., 2018. Degassing-induced fractionation of multiple sulphur isotopes unveils post-Archaean recycled oceanic crust signal in hotspot lava. Nat. Commun. 9 (1), 1–12. https://doi.org/10.1038/s41467-018-07527-w.

Befus, K.S., Walowski, K.J., Hervig, R.L., Cullen, J.T., 2020. Hydrogen isotope composition of a large silicic magma reservoir preserved in quartz-Hosted Glass inclusions of the bishop tuff plinian eruption. Geochem. Geophys. Geosyst. 21 (12) https://doi.org/10.1029/2020GC009358 e2020GC009358.

Black, B.A., Hauri, E.H., Elkins-Tanton, L.T., Brown, S.M., 2014. Sulfur isotopic evidence for sources of volatiles in Siberian Traps magma. Earth Planet. Sci. Lett. 394, 58–69. https://doi.org/10.1016/j.epsl.2014.02.057.

Botcharnikov, R.E., Koepke, J., Holtz, F., McCammon, C., Wilke, M., 2005. The effect of water activity on the oxidation and structural state of Fe in a ferro-basaltic melt. Geochim. Cosmochim. Acta 69 (21), 5071–5085. https://doi.org/10.1016/j.gca.2005.04.023.

Carroll, M.R., Rutherford, M.J., 1988. Sulfur speciation in hydrous experimental glasses of varying oxidation state; results from measured wavelength shifts of sulfur X-rays. Am. Mineral. 73 (7–8), 845–849.

de Moor, J.M., Fischer, T., Sharp, Z., King, P., Wilke, M., Botcharnikov, R.E., Cottrell, E., Zelenski, M., Marty, B., Klimm, K., et al., 2013. Sulfur degassing at Erta Ale (Ethiopia) and Masaya (Nicaragua) volcanoes: Implications for degassing processes and oxygen fugacities of basaltic systems. Geochem. Geophys. Geosyst. 14 (10), 4076–4108. https://doi.org/10.1002/ggge.20255.

Deloule, E., Albarede, F., Sheppard, S.M., 1991. Hydrogen isotope heterogeneities in the mantle from ion probe analysis of amphiboles from ultramafic rocks. Earth Planet. Sci. Lett. 105 (4), 543–553. URL. https://doi.org/10.1016/0012-821X(91)90191-J.

Ding, T., Valkiers, S., Kipphardt, H., De Bievre, P., Taylor, P., Gonfiantini, R., Krouse, R., 2001. Calibrated sulfur isotope abundance ratios of three IAEA sulfur isotope reference materials and V-CDT with a reassessment of the atomic weight of sulfur. Geochim. Cosmochim. Acta 65 (15), 2433–2437. URL. https://doi.org/10.1016/S0016-7037(01)00611-1.

Eiler, J.M., Graham, C., Valley, J.W., 1997. SIMS analysis of oxygen isotopes: matrix effects in complex minerals and glasses. Chem. Geol. 138 (3–4), 221–244. URL. https://doi.org/10.1016/S0009-2541(97)00015-6.

Evans, K., 2012. The redox budget of subduction zones. Earth Sci. Rev. 113 (1), 11–32. https://doi.org/10.1016/j.earscirev.2012.03.003.

Farquhar, J., Wing, B., McKeegan, K., Harris, J., Cartigny, P., Thiemens, M., 2002. Mass-independent sulfur of inclusions in diamond and sulfur recycling on early Earth. Science 298 (5602), 2369–2372. https://doi.org/10.1126/science.1078617.

Fiege, A., Holtz, F., Shimizu, N., Mandeville, C.W., Behrens, H., Knipping, J.L., 2014. Sulfur isotope fractionation between fluid and andesitic melt: an experimental study. Geochim. Cosmochim. Acta 142, 501–521. https://doi.org/10.1016/j.gca.2014.07.015.

Fitzsimons, I.C.W., Harte, B., Clark, R.M., 2000. SIMS stable isotope measurement: counting statistics and analytical precision. Mineral. Mag. 64 (1), 59–83.

Fortin, M.-A., Watson, E.B., Stern, R.A., Ono, S., 2019. Experimental characterization of diffusive and Soret isotopic fractionation of sulfur in a reduced, anhydrous basaltic melt. Chem. Geol. 510, 10–17. https://doi.org/10.1016/j.chemgeo.2019.02.008.

Fukuda, K., Beard, B.L., Dunlap, D.R., Spicuzza, M.J., Fournelle, J.H., Wadhwa, M., Kita, N.T., 2020. Magnesium isotope analysis of olivine and pyroxene by SIMS: Evaluation of matrix effects. Chem. Geol. 119482 https://doi.org/10.1016/j.chemgeo.2020.119482.

Füri, E., Hilton, D., Halldórsson, S., Barry, P., Hahm, D., Fischer, T., Grönvold, K., 2010. Apparent decoupling of the He and Ne isotope systematics of the Icelandic mantle: The role of He depletion, melt mixing, degassing fractionation and air interaction. Geochim. Cosmochim. Acta 74 (11), 3307–3332. https://doi.org/10.1016/j.gca.2010.03.023.

Gurenko, A.A., Chaussidon, M., Schmincke, H.-U., 2001. Magma ascent and contamination beneath one intraplate volcano: evidence from s and o isotopes in glass inclusions and their host clinopyroxenes from miocene basaltic hyaloclastites southwest of gran canaria (canary islands). Geochim. Cosmochim. Acta 65 (23), 4359–4374. https://doi.org/10.1016/S0016-7037(01)00737-2.

Halldórsson, S.A., Barnes, J.D., Stefánsson, A., Hilton, D.R., Hauri, E.H., Marshall, E.W., 2016a. Subducted lithosphere controls halogen enrichments in the Iceland mantle plume source. Geology 44 (8), 679–682. https://doi.org/10.1130/G37924.1.

Halldórsson, S.A., Hilton, D.R., Barry, P.H., Füri, E., Grönvold, K., 2016b. Recycling of crustal material by the Iceland mantle plume: New evidence from nitrogen elemental and isotope systematics of subglacial basalts. Geochim. Cosmochim. Acta 176, 206–226. https://doi.org/10.1016/j.gca.2015.12.021.

Hartley, M., Thordarson, T., Taylor, C., Fitton, J., et al., 2012. Evaluation of the effects of composition on instrumental mass fractionation during SIMS oxygen isotope analyses of glasses. Chem. Geol. 334, 312–323. https://doi.org/10.1016/j.chemgeo.2012.10.027.

Hauri, E., 2002. SIMS analysis of volatiles in silicate glasses, 2: isotopes and abundances in Hawaiian melt inclusions. Chem. Geol. 183 (1–4), 115–141. https://doi.org/10.1016/S0009-2541(01)00374-6.

Hauri, E.H., Shaw, A.M., Wang, J., Dixon, J.E., King, P.L., Mandeville, C., 2006. Matrix effects in hydrogen isotope analysis of silicate glasses by SIMS. Chem. Geol. 235 (3–4), 352–365. https://doi.org/10.1016/j.chemgeo.2006.08.010.

Hinton, R.W., 1995. Ion microprobe analysis in geology. In: Microprobe techniques in the earth sciences. Mineralogical Society Series Volume 6. Chapman & Hall, London.

Ireland, T.R., 2004. Chapter 30 - sims measurement of stable isotopes. In: de Groot, P.A. (Ed.), Handbook of Stable Isotope Analytical Techniques. Elsevier, Amsterdam, pp. 652–691. https://doi.org/10.1016/B978-044451114-0/50032-6.

Jégo, S., Dasgupta, R., 2014. The fate of sulfur during fluid-present melting of subducting basaltic crust at variable oxygen fugacity. J. Petrol. 55 (6), 1019–1050. https://doi.org/10.1093/petrology/egu016.

Labidi, J., Cartigny, P., Moreira, M., 2013. Non-chondritic sulphur isotope composition of the terrestrial mantle. Nature 501 (7466), 208–211. https://doi.org/10.1038/nature12490.

Lange, R.A., 1997. A revised model for the density and thermal expansivity of K_2O - Na_2O - CaO - MgO - Al_2O_3 - SiO_2 liquids from 700 to 1900 K: extension to crustal magmatic temperatures. Contrib. Mineral. Petrol. 130 (1), 1–11. https://doi.org/10.1007/s004100050345.

Lareau, R., Williams, P., 1985. Survey of alkali primary ion sources for SIMS. In: Benninghoven, A., Colton, R.J., S, D., H, W. (Eds.), Secondary Ion Mass Spectrometry, SIMS V. Springer Verlag, Berlin, Berlin, pp. 149–151.

Le Bas, M.J., Le Maitre, R.W., Streckeisen, A., Zanettin, B., 1986. A Chemical Classification of Volcanic Rocks Based on the Total Alkali-Silica Diagram. J. Petrol. 27 (3), 745–750. https://doi.org/10.1093/petrology/27.3.745.

Liotta, M., Rizzo, A., Paonita, A., Caracausi, A., Martelli, M., 2012. Sulfur isotopic compositions of fumarolic and plume gases at mount etna (italy) and inferences on their magmatic source, Geochemistry, Geophysics. Geosystems 13 (5). https://doi.org/10.1029/2012GC004118.

Longpré, M.-A., Stix, J., Klügel, A., Shimizu, N., 2017. Mantle to surface degassing of carbon- and sulphur-rich alkaline magma at El Hierro, Canary Islands. Earth Planet. Sci. Lett. 460, 268–280. https://doi.org/10.1016/j.epsl.2016.11.043.

Manzini, M., Bouvier, A.-S., Barnes, J.D., Bonifacie, M., Rose-Koga, E.F., Ulmer, P., Métrich, N., Bardoux, G., Williams, J., Layne, G.D., et al., 2017. SIMS chlorine isotope analyses in melt inclusions from arc settings. Chem. Geol. 449, 112–122. https://doi.org/10.1016/j.chemgeo.2016.12.002.

Marini, L., Moretti, R., Accornero, M., 2011. Sulfur Isotopes in Magmatic-Hydrothermal Systems, Melts, and Magmas. Rev. Mineral. Geochem. 73 (1), 423–492. https://doi.org/10.2138/rmg.2011.73.14.

Mercier, M., Di Muro, A., Métrich, N., Giordano, D., Belhadj, O., Mandeville, C.W., 2010. Spectroscopic analysis (FTIR, Raman) of water in mafic and intermediate glasses and glass inclusions. Geochim. Cosmochim. Acta 74 (19), 5641–5656. https://doi.org/10.1016/j.gca.2010.06.020.

Michel, A., Villemant, B., 2003. Determination of Halogens (F, Cl, Br, I), Sulfur and Water in Seventeen Geological Reference Materials. Geostand. Newslett. 27 (2), 163–171. https://doi.org/10.1111/j.1751-908X.2003.tb00643.x.

Moussallam, Y., Morizet, Y., Gaillard, F., 2016. H_2O–CO_2 solubility in low SiO_2-melts and the unique mode of kimberlite degassing and emplacement. Earth Planet. Sci. Lett. 447, 151–160. https://doi.org/10.1016/j.epsl.2016.04.037.

Moussallam, Y., Longpré, M.-A., McCammon, C., Gomez-Ulla, A., Rose-Koga, E.F., Scaillet, B., Peters, N., Gennaro, E., Paris, R., Oppenheimer, C., 2019. Mantle plumes are oxidised. Earth Planet. Sci. Lett. 527, 115798. https://doi.org/10.1016/j.epsl.2019.115798.

Nash, W.M., Smythe, D.J., Wood, B.J., 2019. Compositional and temperature effects on sulfur speciation and solubility in silicate melts. Earth Planet. Sci. Lett. 507, 187–198. https://doi.org/10.1016/j.epsl.2018.12.006.

Ono, S., Keller, N.S., Rouxel, O., Alt, J.C., 2012. Sulfur-33 constraints on the origin of secondary pyrite in altered oceanic basement. Geochim. Cosmochim. Acta 87, 323–340. https://doi.org/10.1016/j.gca.2012.04.016.

Óskarsson, N., Helgason, Ö., Steinthórsson, S., 1994. Oxidation state of iron in mantle-derived magmas of the Icelandic rift zone. Hyperfine Interactions 91 (1), 733–737. https://doi.org/10.1007/BF02064599.

Ranta, E., Gunnarsson-Robin, J., Halldórsson, S. A., Ono, S., Izon, G., Jackson, M. G., Reekie, C. D. J., Jenner, F. E., GuÃ°finnsson, G. H., Jónsson, O. P., Stefánsson, A., in review. Primordial and recycled sulfur sampled by the Iceland mantle plume, Earth Planet. Sci. Lett.

Rosner, M., Wiedenbeck, M., Ludwig, T., 2008. Composition-Induced Variations in SIMS Instrumental Mass Fractionation during Boron Isotope Ratio Measurements of Silicate Glasses. Geostand. Geoanal. Res. 32 (1), 27–38. https://doi.org/10.1111/j.1751-908X.2008.00875.x.

Sasaki, A., Arikawa, Y., Folinsbee, R., 1979. Kiba reagent method of sulfur extraction applied to isotopic work. Chishitsu Chosajo Geppo 30 (4), 241–245.

Schauble, E.A., 2004. Applying stable isotope fractionation theory to new systems. Rev. Mineral. Geochem. 55 (1), 65–111. https://doi.org/10.2138/gsrmg.55.1.65.

Schuessler, J.A., Botcharnikov, R.E., Behrens, H., Misiti, V., Freda, C., 2008. Amorphous Materials: Properties, structure, and durability: Oxidation state of iron in hydrous phono-tephritic melts. Am. Mineral. 93 (10), 1493–1504. https://doi.org/10.2138/am.2008.2795.

Seo, J.H., Guillong, M., Heinrich, C.A., 2009. The role of sulfur in the formation of magmatic–hydrothermal copper–gold deposits. Earth Planet. Sci. Lett. 282 (1), 323–328. https://doi.org/10.1016/j.epsl.2009.03.036.

Shimizu, K., Ushikubo, T., Murai, T., Matsu'ura, F., Ueno, Y., 2019. In situ analyses of hydrogen and sulfur isotope ratios in basaltic glass using sims. Geochem. J. 53 (3), 195–207. https://doi.org/10.2343/geochemj.2.0559.

Shorttle, O., Moussallam, Y., Hartley, M.E., Maclennan, J., Edmonds, M., Murton, B.J., 2015. Fe-XANES analyses of Reykjanes Ridge basalts: Implications for oceanic crust's role in the solid Earth oxygen cycle. Earth Planet. Sci. Lett. 427, 272–285. https://doi.org/10.1016/j.epsl.2015.07.017.

Simon, A.C., Ripley, E.M., 2011. The Role of Magmatic Sulfur in the Formation of Ore Deposits. Rev. Mineral. Geochem. 73 (1), 513–578. https://doi.org/10.2138/rmg.2011.73.16.

Śliwiński, M.G., Kitajima, K., Spicuzza, M.J., Orland, I.J., Ishida, A., Fournelle, J.H., Valley, J.W., 2018. SIMS Bias on Isotope Ratios in Ca-Mg-Fe Carbonates (Part III): $\delta^{18}O$ and $\delta^{13}C$ Matrix Effects Along the Magnesite–Siderite Solid-Solution Series. Geostand. Geoanal. Res. 42 (1), 49–76. https://doi.org/10.1111/ggr.12194.

Vielzeuf, D., Champenois, M., Valley, J.W., Brunet, F., Devidal, J., 2005. SIMS analyses of oxygen isotopes: matrix effects in Fe–Mg–Ca garnets. Chem. Geol. 223 (4), 208–226. https://doi.org/10.1016/j.chemgeo.2005.07.008.

Walters, J., Cruz-Uribe, A., Marschall, H., 2020. Sulfur loss from subducted altered oceanic crust and implications for mantle oxidation. Geochem. Perspectiv. Lett. 13, 36–41. https://doi.org/10.7185/geochemlet.2011.

Wilke, M., Klimm, K., Kohn, S.C., 2011. Spectroscopic studies on sulfur speciation in 1034 synthetic and natural glasses. Rev. Mineral. Geochem. 73 (1), 41–78. https://doi.org/10.2138/rmg.2011.73.3, 1035.